Insights into characteristics, sources and evolution of submicron aerosols during harvest seasons in Yangtze River Delta (YRD) region, China

Y. J. Zhang[1,2], L. L. Tang[2,1], Z. Wang[1], H. X. Yu[3], Y. L. Sun[4], D. Liu[5], W. Qin[2], F. Canonaco[6], A. S. H. Prévôt[6], H. L. Zhang[7], and H.-C. Zhou[1]

[1]Jiangsu Key Laboratory of Atmospheric Environment Monitoring and Pollution Control, School of Environmental Science and Engineering, Nanjing University of Information Science and Technology, Nanjing 210044, China

[2]Jiangsu Environmental Monitoring Center, Nanjing 210036, China

[3]State key laboratory of Pollution Control and Resource Reuse, School of the Environment, Nanjing University, Nanjing 210093, China

[4]State Key Laboratory of Atmospheric Boundary Layer Physics and Atmospheric Chemistry, Institute of Atmospheric Physics, Chinese Academy of Sciences, Beijing 100029, China

[5]Centre for Atmospheric Science, School of Earth, Atmospheric and Environmental Sciences, University of Manchester, Manchester M13 9PL, UK

[6]Laboratory of Atmospheric Chemistry, Paul Scherrer Institute, Villigen PSI 5232, Switzerland

[7]Handix LLC, Boulder, CO 8031, USA

Correspondence to: L. L. Tang (lily3258@163.com)

Abstract

Atmospheric submicron particulate matter (PM_1) is one of the most significant pollution components in China. Despite its current popularity in the studies of aerosol chemistry, the characteristics, sources and evolution of atmospheric PM_1 species are still poorly understood in China, particularly for the two harvest seasons, namely the summer wheat harvest and autumn rice harvest. An Aerodyne Aerosol Chemical Speciation Monitor (ACSM) was deployed for online monitoring of PM_1 components during summer and autumn harvest seasons in urban Nanjing, a megacity in the Yangtze River Delta (YRD) region of China. PM_1 components were shown to be dominated by organic fraction (OA, 39% and 41%) and nitrate (23% and 20%) during the harvest seasons (the summer and autumn harvest). Positive matrix factorization (PMF) analysis of the ACSM OA mass spectra resolved four OA factors: hydrocarbon-like mixed with cooking related OA (HOA + COA), fresh biomass burning OA (BBOA), oxidized biomass burning-influenced OA (OOA-BB), and highly oxidized OA (OOA); in particular the oxidized BBOA dominates ~80% of the total BBOA loadings. Both fresh and oxidized BBOA exhibited apparent diurnal cycles with peak concentration at night, when the high ambient relative humidity and low temperature facilitated the formation of semi-volatile organic species. The BBOA concentrations for the harvests are estimated as BBOA = 15.1 × (*m/z* 60 – 0.26% × OA), *m/z* 60 as a marker for levoglucosan-like species. The OA mass decreases with the aging of BB plumes, indicating that the fresh BB plumes contribute to the OA burden significantly. Analysis of air masses back-trajectory indicates that the high BB pollutants are linked to the air masses from the western (summer harvest) and southern (autumn harvest) areas.

1 Introduction

Particulate matter (PM) that is suspended in the atmosphere as atmospheric aerosol plays a

crucial role in regional and global climate system (Ramanathan et al., 2001; Kaufman et al., 2002), air pollution (Sun et al., 2013), ambient visibility reduction (Watson, 2002) and human health (Ge et al., 2011). Significant amounts of PM can be generated from human activities. In particular, biomass burning (BB) activities, e.g., forest fires, wildfire, and agricultural fires, can become the main sources of fine particulate matter ($PM_{2.5}$, particulates $\leq$ 2.5 μm in aerodynamic diameter) and/or submicron particulate matter (PM_1, particulates $\leq$ 1 μm in aerodynamic diameter) (Andreae and Merlet, 2001, Aiken et al., 2010; DeCarlo et al., 2010; Lee et al., 2010; Cubison et al., 2011; Reche et al., 2012; Bougiatioti et al., 2013). Agricultural residues burning is one of the most serious sources leading to severe air quality problems during harvest seasons in China (Li et al., 2007; Wang et al., 2009a; Du et al., 2011; Cheng et al., 2013; Ding et al., 2013). Moreover, China is an agricultural country which has 1.8 billion cultivated fields with a large number of agricultural crop residue (Zhang et al., 2008). Recently, the use of agricultural residues as fuel in China declined. During harvest seasons, farmers usually harvest the crop in the daytime and burn agricultural residues in their fields in the nighttime directly, which may result in BB emission. The understanding of the compositions, sources and processes of atmospheric aerosol particles during harvest seasons is urgently needed to design measures to improve the quality of air in China.

Organic aerosol (OA) composes a large fraction of atmospheric aerosol particles (Zhang et al., 2007). Combination of positive matrix factorization (PMF, Paatero, 1997) and a PMF Evaluation Toolkit (PET, Ulbrich et al., 2009) has been well used to identify the sources apportionment of OA in recent studies (e.g. Lanz et al., 2007; Ulbrich et al., 2009; Allan et al., 2010; Zhang et al., 2005a, 2011; Crippa et al., 2013, 2014; Sun et al., 2013). In addition, an IGOR-based Source Finder (SoFi, Canonaco et al., 2013) with a multilinear engine algorithm (ME-2, Paatero, 1999) can also resolve the emission sources of OA. The current PMF and ME-2 method can only be employed to analyze OA datasets a posteriori (Sun et al., 2012;

Zhang et al., 2011; Canonaco et al., 2013), but cannot be easily utilized in the real-time online estimation of atmospheric OA sources. To identify the sources of atmospheric OA online, an algorithm based solely on organic mass fragments, namely *m/z* 57 (mostly $C_4H_9^+$) and *m/z* 44 (mostly CO_2^+), were developed to estimate hydrocarbon-like OA (HOA) and oxygenated OA (OOA), respectively (Zhang et al., 2005a; 2005b; Ng et al., 2011c). Mohr et al. (2012) also identified cooking OA (COA) in ambient datasets based on the fractions of COA tracers at *m/z* 55 (mostly $C_4H_7^+$) and *m/z* 57 organic mass fragments. Biomass burning organic aerosol (BBOA) is one of the major atmospheric OA species during BB periods (Aiken et al., 2010; Allan et al., 2010). However, limited information is available for estimating the source appointments of BBOA.

The evolution of atmospheric OA such as oxidation process can significantly influence the ambient concentrations and physicochemical properties of OA (Aiken et al., 2008; Jimenez et al., 2009; Sun et al., 2011b). In the presence of BB source, various volatile and semi-volatile organic precursors can be emitted from the field burning of agricultural wastes, and SOA can be formed from these precursors rapidly (Jimenez et al. 2009; Grieshop et al., 2009; Heringa et al., 2011; Kawamura et al., 2013). What is more, BB plumes can be mixed with urban and regional pollutants during aging processes (DeCarlo et al., 2010; Cubison et al., 2011). In addition to source emissions, the secondary formation, atmospheric transport and diffusion, as well as the mass loadings and oxidation state of ambient OA can be also affected by the aging processes of OA (Jimenez et al., 2009; Cubison et al., 2011; Sun et al., 2011b). Thus, it is important for understanding the nature of atmospheric OA to investigate the evolution of OA and the evolution process effects.

This study investigates the characteristics of PM_1 species using an Aerodyne Aerosol Chemical Speciation Monitor (ACSM), and OA mass spectra is resolved with PMF model during summer and autumn harvests in the YRD region; the evolution of OA and the effects

of the evolution process on PM burden were also investigated. Combination of back-trajectory analysis and local wind meteorology was used to investigate the source origins.

2 Experimental methods

2.1 Sampling site description

With a population of more than 8 million and an area of about 6597 km^2, Nanjing, a megacity, is a representative Chinese city in terms of the pollution characteristics of the YRD region. Local and regional air pollution events frequently occur in Nanjing, mainly caused by emissions of mixed aerosols from fossil fuel burning, residential activities, and agricultural residues burning (Wang et al., 2009a; Ding et al., 2013). In this study, all kinds of data was collected in urban Nanjing (118°46'N, 32°05'E) from June 1 to 15, and October 15 to 30, 2013, corresponding to two harvest seasons in a year, namely the summer wheat harvest and autumn rice harvest. In this study, the sampling site was located on the roof of a six-story building approximately 18 m above ground level, ~15 m from the nearest heavy-traffic road, and ~50 m from the nearest restaurants and residents. As a matter of fact, there is no agricultural field in the urban Nanjing areas. This means that the urban Nanjing site is significantly influenced by the BB plumes originated the rural areas and undergone the aging in BB plumes measured dozens or hundreds of kilometers away from the fire locations, but is little/negligible influenced by the local BB. In addition, the local cooking and traffic emissions can also significantly affect the PM pollution in this sampling site. Therefore, in the presence of BB plumes, the mixed/complicated air pollution will occur in urban Nanjing during the harvest seasons.

2.2 Instrumentation and data analysis

2.2.1 Measurements

The ambient NR-PM_1 species, i.e., OA, nitrate, sulfate, ammonium, chloride, were continuously measured using ACSM from June 1 to 15, and October 15 to 30, 2013. Detailed descriptions of ACSM can be found in previous studies (Ng et al., 2011a; Sun et al., 2012). Briefly, the ambient aerosols were drawn into the room using a ½ inch (outer diameter) stainless steel tube at a flow rate of ~3 L min^{-1}, of which ~84 cc min^{-1} was sub-sampled into the ACSM. Moreover, ACSM was operated at a time resolution of about 15 min with a scan from *m/z* 10 to 150 amu at 500 ms amu^{-1} rate, which corresponds to the settings of Sun et al. (2012).

An online analyzer, Monitoring of Aerosols and Gases (MARGA, model ADI 2080 Applikon Analytical B. V. Corp., the Netherlands), was deployed to measure the mass concentrations of a major water-soluble inorganic ion (potassium ion, K^+) in the aerosols. A $PM_{2.5}$ cyclone inlet was used to remove coarse particles. Ambient air was sampled into a liquid with a flow rate of 16.7 L min^{-1}. The detection limits of K^+ is 0.09 μg m^{-3}. The MET ONE BAM-1020 and the 7-wavelength aethalometer (Magee AE31) were also employed to measure PM_1 and ambient atmospheric BC in $PM_{2.5}$, respectively. CO was measured using an gas analyzer (Thermo Scientific, Model 48i). Ambient meteorological parameters including ambient temperature (*T*), relative humidity (RH), precipitation, wind speed (WS), and wind direction (WD) were obtained from a ground meteorology station located on the same six-story building as the sampling site.

Daily fire locations used in this study were available from MODIS (Moderate-resolution Imaging Spectroradiometer) mounted on NASA's Terra and Aqua satellites, NASA's Earth Observing System (EOS) (https://earthdata.nasa.gov/data/near-real-time-data/firms). MODIS can present fire distributions in details at 1 km resolution through Fire Information for

Resource Management System (FIRMS) on global scale (Justice et al., 2002; Kaufman et al., 2003). As shown in Fig. S1 − S2, all agricultural fire locations (red dots) in the YRD region were detected by the remote sensing retrieval of MODIS from June 1 to 15, and October 15 to 30, 2013 (https://firms.modaps.eosdis.nasa.gov/firemap/).

2.2.2 ACSM data analysis

An ACSM Data Analysis Software package, ACSM Local (Ver. 1.5.2.0.0, released April 25, 2012) written in Wavemetrics Igor^{TM}, was used to analyze the ACSM dataset. More details of procedures have been described in the studies of Ng et al. (2011a) and Sun et al. (2012). The ACSM calibration is based on a combination of a Differential Mobility Analyzer (DMA, TSI model 3080) and Condensation Particle Counter (CPC, TSI model 3775) for the ionization efficiency (IE) and relative ionization efficiencies (RIEs). And the pure ammonium nitrate (NH_4NO_3) particles (size selected by 300 nm) are used for the quantitative measurements, because NH_4NO_3 vaporizes with 100% efficiency (Ng et al., 2011a). The RIEs values usually used in Aerosol Mass Spectrometer (AMS) ambient concentration calculations (Canagaratna et al., 2007) are the default values of organics (1.4), nitrate (1.1), sulfate (1.2), and chloride (1.3) in this study. Moreover, a RIE value of ammonium is 7.04, and the response factor (RF) value of nitrate is 3.96×10^{-11} in this study. In addition, the mass concentrations of ambient aerosol need to be corrected for particle collection efficiency (CE) (Middlebrook et al., 2011). CE = 0.5 is found to be representative with data uncertainties generally within 20% (Canagaratna et al., 2007; Middlebrook et al., 2011). The CE values observed in previous studies range from 0.43 to 1, due to (a) shape-related collection losses at the vaporizer from inefficient focusing of non-spherical particles, (b) particle losses at the vaporizer because of bouncing of solid particles before they are completely vaporized, and (c) particle losses in the aerodynamic inlet as a function of particle diameter (Allan et al., 2004; Zhang et al., 2005b;

171 Canagaratna et al. 2007; Middlebrook et al., 2011). In this study, we selected the CE value
172 for OA, nitrate, sulfate, ammonium, and chloride, respectively, according to the equation CE
173 = max (0.45, 0.0833 + 0.9167 × ANMF) (Middlebrook et al., 2011), in which ANMF is the
174 mass fraction of NH_4NO_3 measured by the ACSM.

175 The PMF method was also applied to analyze OA datasets from the ACSM. More details
176 of procedure for the PMF model can be found in previous studies (Ulbrich et al., 2009; Zhang
177 et al., 2005a, 2011). Furthermore, the OA mass spectra data from the ACSM were determined
178 by combing PMF2 executables with the PMF Evaluation Tool (PET) (Ulbrich et al., 2009).
179 Due to large interferences of internal standard of naphthalene at *m/z*'s 127 − 129, the PMF
180 analysis was restricted to *m/z* 120 (Sun et al., 2012, 2013). Based on the OA dataset from the
181 ACSM, the PMF analysis was performed for 1 to 7 factors. A summary of the PMF results is
182 presented in Figure S6 − S15. For the chosen number of factors, fpeaks were varied in steps
183 of 0.1 from −1 to 1 during the summer and autumn harvest. Four OA factors, i.e.,
184 hydrocarbon-like mixed with cooking OA (HOA + COA), fresh biomass-burning OA
185 (BBOA), oxidized BB-influenced OA (OOA-BB), and highly oxygenated OA (OOA) were
186 resolved in this study. The HOA + COA was considered as a factor mixing with COA and
187 traffic HOA in the 4-factor solution, while the "HOA + COA" factor splits into factors with
188 very similar time series in the five- to a seven-factor solution. This means that the PMF
189 analysis of the ACSM OA mass spectra is difficult to distinguish the COA from the traffic
190 HOA in this study. Sun et al. (2010) and Sun et al. (2012) also found a similar phenomenon
191 for distinguishing COA from traffic HOA in a Quadrupole AMS (Q-AMS) and an ACSM
192 OA mass spectra using PMF analysis in Beijing. However, the PMF analysis of high
193 resolution OA mass spectra measured by a high-resolution time-of-flight aerosol mass
194 spectrometer (HR-ToF-AMS) was able to distinguish the COA from the traffic HOA and
195 COA (Huang et al., 2010). For the 3-factor solution, BBOA might be mixed with OOA-BB,

while the 4-factor solution (which contained two BB-related BBOA factors, i.e., BBOA and OOA-BB) seemed to be valid (more details can be found in section 3.2). Recent studies also found the highly similar results with PMF analysis of the OA mass spectra in field studies (Crippa et al., 2013; Bougiatioti et al., 2014; Young et al., 2014). The detailed lists of explanation on the reasons for the selection of the 4-factor solution can be found in Table S4 − S5. In addition, the OA source apportionment for the two harvests will be further discussed in section 3.2.

2.2.3 Back-trajectory analysis

Impacts of various source regions on the PM pollution during the harvest seasons have been investigated using the HYbrid Single Particle Lagrangian Integrated Trajectory (HYSPLIT-4) model developed by NOAA/ARL (Draxler and Rolph, 2003). Accordingly, 48 h back-trajectories at 500 m arrival height above ground level were calculated every 2 h starting at China Standard Time (CST) based on a Trajectory Statistics (TrajStat) software developed by Wang et al. (2009b). In this study, the 48 h back-trajectories of air masses were used for further analysis.

3 Results and discussion

3.1 Meteorological factors and PM_1 components

3.1.1 Time series of meteorological factors and PM_1 components

Figure 1 shows the time series of NR-PM_1 species and BC in the presence of different meteorological conditions during the harvest seasons in urban Nanjing, i.e., WS, WD, RH, *T*, and precipitation. During the summer harvest, the average values were 70.7 ± 15.3%, 3.7 ± 1.7 m s^{-1}, and 23.4 ± 4.1 ℃ for the ambient RH, WS, and *T*, respectively. In the autumn harvest, the average values were 54.3 ± 13.7 %, 2.6 ± 1.4 m s^{-1}, and 18.1 ± 3.6 ℃ for the

ambient RH, WS, and *T*, respectively. The frequency distribution of hourly averaged wind direction and speed throughout the summer and autumn harvests were shown in Figure S2 (a – b).

As shown in Figure S3, there is a strong correlation between the MET ONE PM_1 measured by MET ONE BAM-1020 and the PM_1 (= NR-PM_1 + BC) mass concentrations (r^2 = 0.88, *slope* = 1.11), indicating that the ambient submicron aerosols consisted mainly of the NR-PM_1 and BC. Note that the mass concentration of BC in the PM_1 may be overestimated due to the fact that the mass concentration of BC was measured by the 7-wavelength aethalometer for $PM_{2.5}$ and the uncertainties in converting measured light absorption coefficients to carbon concentrations. An overestimation was previously suggested by Huang et al. (2011). The average PM_1 mass for the summer harvest is 38.5 μg m^{-3} with hourly average ranging from 3.6 to 270.6 μg m^{-3}, which is similar to that observed in the autumn harvest (42.3 μg m^{-3}) with hourly average ranging 8.1 to 191.5 μg m^{-3}. Indeed, PM_1 consisted of OA (39%), nitrate (23%), ammonium (16%), sulfate (12%), BC (8%), and chloride (1%) during the summer harvest. During the autumn harvest, PM_1 was composed of OA (41%), nitrate (20%), ammonium (14%), sulfate (11%), BC (13%), and chloride (1%). Table 1 presents a comparison of the average composition of PM_1 between the summer harvest and autumn harvest periods. The average bulk composition of PM_1 during the summer harvest shows similar dominance of OA to the PM pollution during the autumn harvest, but lower mass fractions for other species except nitrate. This is also consistent with some previous findings in the presence of BB source emissions (Crippa et al., 2013; Huang et al., 2013; Bougiatioti et al., 2014). Overall, those species also show a similar contribution between the summer and autumn harvest to the PM_1 mass, suggesting that the PM pollution could be affected by similar pollution sources for the two harvests.

As shown in Fig. 1, all aerosol species exhibited very dynamic variations in mass concentrations due to the changes of source emissions, meteorology factors (such as RH, *T*, and planetary boundary layer height), photochemical reactions and regional transport (e.g. the BB plumes). For example, the aerosol species dramatically reduced because of the quick removal processes associated with heavy wet scavenging and/or the dilution of the atmosphere (e.g. 6 – 8 June) during the summer harvest. However, the wet scavenging plays a minor role in changing aerosol loadings with little precipitation during the autumn harvest. OA shows a significant dynamic variation in mass concentrations during the harvest seasons (Fig. 1c), likely due to the changes of source emissions (such as cooking, traffic and/or BB emissions). There are three sharp peaks during the summer harvest (case 1) and autumn harvest (case 2 and case 3). The relationships between the PM pollution, meteorology and chemical composition are presented in three case events (Table S1). The case 1, at 21:00 – 22:00 on 10 June, with the highest PM_1 mass (253.1 μg m^{-3}) can be associated with the northwest wind at 2.5 m s^{-1}. Due to long-range transported pollutants from agricultural fires in the summer harvest (Figure S1), the PM pollution should be affected by the BB plumes from the northwest areas around the urban Nanjing. This speculation is consistent with the highest loadings of K^+, BBOA, OOA-BB, chloride, and BC during the summer harvest. Thus, the case 1 was mainly affected by the BB plumes. Apart from the high loadings of BBOA, OOA-BB, BC, and K^+ show in the case 2 and case 3 periods, HOA + COA also presents the high concentrations. This suggests that both local primary sources emission and regional BB plumes dominate the PM pollution during the case 2 and case 3 periods. Therefore, those findings indicate that indeed BB contributes significantly in the area during the specific time period.

3.1.2 Diurnal variations of meteorological factors and PM_1 components

Figure 2 depicts the diurnal variations of the meteorological factors, i.e., RH, *T*, and WS, and PM_1 species (including OA, nitrate, sulfate, ammonium, chloride, and BC). Generally, the diurnal variations of the meteorological parameters and PM_1 species are similar during the summer and autumn harvest. However, the ambient RH and *T* during summer harvest were higher than those during autumn harvest. OA obviously exhibits three peaks occurring between 6:00 – 8:00, 11:00 – 14:00, and 19:00 – 22:00, which is in agreement with the emission behaviors of pollution sources, i.e., traffic, cooking and/or BB emissions (Allan et al., 2010; Huang et al., 2012; Sun et al., 2012; Crippa et al., 2013). More details of the diurnal variations of the OA components will be presented in section 3.2.

Sulfate presents a weaker diurnal variation during both summer and autumn harvest, and shows a similar concentration during the two harvests. This means the non-volatile and character of sulfate and its more regional pollution in the YRD region during the summer and autumn harvest. Similar diurnal trend of sulfate was also found by Huang et al. (2012) in the eastern YRD region. Nitrate presents in a higher fraction of the total PM_1 compared with sulfate, yet with lower concentrations in the afternoon and higher concentrations in the evening during the harvests. Similarly, nitrate also shows a similar concentration for the two harvests during the whole day. In addition, chloride shows a similar diurnal cycle with nitrate during the two harvest seasons. This is in accordance with the volatile properties of ammonium nitrate and ammonium chloride dependent on ambient *T* and RH (Lanz et al., 2007; Sun et al., 2011b, 2012). This also reflects that the photochemical production of HNO_3 cannot compensate for the evaporative loss at the relatively high *T* conditions during the two harvests, which is similar to previous results observed by Huang et al. (2012) in the eastern YRD region and Sun et al. (2012) in Beijing. Furthermore, the higher boundary layer may dilute their loadings during the daytime, and then influence their diurnal cycles (Sun et al.,

2012). Chloride is mainly ammonium chloride (NH_4Cl) and/or organic chlorine-containing species (Huffman et al., 2009; Huang et al., 2012; Sun et al., 2012). During the harvest seasons, the evening high values of nitrate and chloride might be affected by the BB emissions and/or formed via gas-phase and aqueous-phase oxidations.

BC shows a classic diurnal variation with higher loadings appearing in early morning and during nighttime, which is consistent with traffic rush hours in early morning (07:00 – 08:00) and during nighttime (20:00 – 21:00). As previous studies, atmospheric BC is strongly associated with combustion emissions (including traffic and BB sources emissions), particular for BB periods (Sandradewi et al., 2008; Liu et al., 2011, 2014; Crippa et al., 2013). Therefore, the reason for the peak values of BC during the nighttime may be also caused by the BB emissions during the harvest seasons, apart from the effect of traffic source on the BC loadings. The lower concentrations of BC in the afternoon can be associated with the dilution effects of higher planetary boundary layer and reduced traffic emissions.

3.2 Organic source apportionment

Four OA factors (i.e. HOA + COA, BBOA, OOA-BB, and OOA) were identified, as illustrated in Fig. 3 and Fig. 4. The mean mass concentrations of HOA + COA, BBOA, OOA-BB and OOA during the harvest seasons were presented in Table 1. HOA + COA, BBOA, OOA-BB, and OOA accounted on average for 15% (28%), 7% (7%), 29% (33%) and 49% (32%) of the total OA mass concentrations during the summer (autumn) harvest, respectively.

3.2.1 Hydrocarbon-like and cooking-emission related OA (HOA + COA)

The prominent hydrocarbon ion series of $C_nH_{2n+1}^+$ and $C_nH_{2n-1}^+$ (e.g. 27, 29, 41, 43, 55, 57...) obtained from mass spectrum were characterized as the components of HOA (Zhang et al.,

2005a, 2011; Mohr et al. 2009; Allan et al., 2010). As reported in previous studies, *m/z* 57 ($C_3H_5O^+$ and/or $C_4H_9^+$) and *m/z* 55 ($C_3H_3O^+$ and/or $C_4H_7^+$) are commonly considered as tracers for the primary organic emissions of combustion sources in urban areas, including COA and HOA (Zhang et al., 2005a; Ng et al., 2010, 2011b; He et al., 2010; Sun et al., 2012, 2013; Hu et al., 2013). It is found that there is no significant difference in the mass spectrum between the summer harvest and the autumn harvest (Fig. 3a). Compared with traffic-like OA (Liu et al., 2011; Crippa et al., 2013), the mass spectrum obtained in the present study shows a higher *m/z* 55/57 ratio. Previous studies indicated that high *m/z* 55/57 together with a unique diurnal variation can be used as a diagnostics for the presence of COA (Mohr et al., 2009; Allan et al., 2010; Sun et al., 2012). The mass spectrum of HOA in this study is characterized by more abundant ions, i.e., *m/z* 41 (mainly $C_3H_5^+$), *m/z* 55 (mainly $C_4H_7^+$) and *m/z* 57 (Fig. 3a), which is similar to the characteristics of COA mass spectrum measured by He et al. (2010). As shown in Fig. 3, the diurnal variation of HOA + COA shows two pronounced peaks corresponding to noon (a weak peak) and evening traffic/cooking activities (a strong peak). Hence, HOA + COA in this study refers to the sum of traffic-related HOA and COA. Similarly, Sun et al. (2010) and Sun et al. (2012) also found that HOA species in urban ambient were influenced by both traffic and cooking-like emissions. In addition, it is seen that the high HOA + COA concentration (> 6 μg m^{-3}) occurred when WD was from southeast during the summer harvest (Fig. S4). During the autumn harvest, the high concentration of HOA + COA was associated with northerly and easterly winds. This result is well consistent with the areas of local cooking and traffic sources emissions around the sampling site.

3.2.2 Fresh biomass burning OA (BBOA)

As shown in Fig. 3b, the mass spectrum of BBOA extracted in this study shows a prominent peak of *m/z* 60 (almost all $C_2H_4O_2^+$) which is a well-known tracer ion for BB emissions

(Alfarra et al., 2007; Aiken et al., 2009; Cubison et al., 2011; Huang et al., 2011; Liu et al., 2011). Levoglucosan was shown to contribute to *m/z* 60 and was found in large amounts in urban, suburban, and rural background atmosphere during BB periods (Maenhaut et al., 2012). In addition, the BBOA is also characterized by higher peaks at masses *m/z* 27, 29, 41, 43, 55, 57, 77 and 91 that are indicative of freshly emitted organic aerosol, because fresh *m/z* 43….. *m/z* 57 can be also from BB-related emissions (Aiken et al., 2009; Heringa et al., 2011; Bougiatioti et al., 2014). For example, primary BBOA (P-BBOA) has a significant contribution from a non-oxygenated ion $C_3H_7^+$ at *m/z* 43, but not from an oxygenated ion $C_2H_3O^+$ (*m/z* 43) in smog chamber experiments by Heringa et al. (2011). The BBOA spectrum profiles with the lack of *m/z* 44 signal (CO_2^+) during the summer and autumn harvest show high correlation (r^2 = 0.82 and r^2 = 0.87) with a result in Paris (Crippa et al., 2013). This spectral pattern also shows much similarity to the spectrum of pure BBOA with the fresh burning condition (flaming phase) in a wood stove (Weimer et al., 2008). Moreover, the spectrum of BBOA in this study is qualitatively similar to published BB spectra from the fresh BB smoke in a smog chamber (Grieshop et al., 2009). These findings suggest that this factor can be related to BBOA with low atmospheric oxidants, and thus this factor might be fresh/primary BBOA during the harvests.

Using soluble K^+ as a tracer for BB has also been reported by previous analyses of BB campaign data (Gilardoni et al., 2009; Aiken et al., 2010; Du et al., 2011; Crippa et al., 2013). The time series of BBOA along with K^+ measured by MARGA is shown in Fig. 4b. BBOA is strongly consistent with K^+ (r^2 = 0.95 and r^2 = 0.75) during the summer and autumn harvest respectively (Fig. 5a), suggesting that BBOA and K^+ were from the same source. In addition, the diurnal variation of BBOA shows a pronounced peak at the nighttime, which is consistent with the effects of the BB emissions (Fig. 3). This means that BBOA contributes to POA during the nighttime mainly. This finding is also consistent with the habit of the farmers in

the YRD region, namely that they usually harvest wheat or rice in the daytime and burn off straw in the nighttime during the harvest seasons each year. In addition, chloride correlates well with BBOA (r^2 = 0.61 and r^2 = 0.66) and K^+ (r^2 = 0.60 and r^2 = 0.64) during the harvest seasons (Figure S5). This means that chloride was mainly from the BB emissions and might be in the form of KCl during the BB periods.

3.2.3 Oxygenated OA (OOA) and oxidized BB-influenced OA (OOA-BB)

The mass spectrum of both OOA components (Fig. 3d) were characterized by the prominent $C_xH_yO_z^+$ fragments, mainly CO_2^+ (*m/z* 44) which has been denoted previously found in many AMS studies (Zhang et al., 2005a; Lanz et al., 2007; Sun et al., 2010; Crippa et al., 2013). The mass spectrums of OOA by the prominent peak of *m/z* 44 (22.9% and 25.5% of the total OOA signal respectively) during the summer and autumn harvest are strongly consistent with more oxidized OOA component determined (r^2 = 0.91 and r^2 = 0.89, Fig. 3d) in BB-period in Paris (Crippa et al., 2013) and OOA components resolved at other urban sites (Lanz et al., 2007; Ulbrich et al., 2009).

As shown in Fig. 4d, the time series of OOA is compared with the sulfate mass loadings. A good correlation was observed between time series of OOA and sulfate mass loadings (r^2 = 0.60 and r^2 = 0.46, Fig. 6) during the summer and autumn harvests, respectively. Previous studies performed at various sites also showed that these two species were secondary with low-volatility property in the atmosphere (Zhang et al., 2005c; Lanz et al., 2007; Ulbrich et al., 2009; Sun et al., 2011a; Huang et al., 2012). Overall, the diurnal pattern of OOA shows relatively stable variation throughout the whole day (Fig. 3). OOA often remains at a high concentration across several days until a change of air mass occurs, which shows a regional production (Sun et al., 2012, 2013). This may be a main reason causing the relatively stable variation thorough the whole day in this study. Nevertheless, OOA shows a slightly increase

394 at around 12:00 – 15:00, suggesting that OOA might be formed by photochemical processing
395 during the daytime in the harvest seasons. OOA also exhibits higher loadings during the
396 nighttime, probably caused by the aging of BB plumes, in which BB emissions will be further
397 oxidized and begin to transition into OOA (Jimenez et al., 2009, DeCarlo et al., 2010). The
398 uniform distribution of its concentrations is almost in association with all kinds of WD during
399 the summer and autumn harvest respectively (Figure S4). This is a good evidence for
400 explaining the regional pollution of OOA in the YRD region during the harvest seasons.

401 Additionally, an oxygenated factor with the high degree of oxygenation during the
402 summer and autumn harvest (*m/z* 44, 18.2% and 14.5% of the total factor signal respectively)
403 in its mass spectrum has been resolved as oxidized BB- influenced OA (OOA-BB, Fig. 3c).
404 The mass spectrums of OOA-BB are characterized by both the oxidized signals (*m/z* 18, 29,
405 43 and 44) and the typical marker of BB (*m/z* 60) during the summer and autumn harvest,
406 which correlates well with BB-emission related OOA (OOA_2-BBOA) (r^2 = 0.85 and r^2=0.86)
407 during BB periods at an urban site in Paris (Crippa et al., 2013). It is also highly similar to the
408 mass spectrum of the aged BBOA identified by DeCarlo et al. (2010) for airborne
409 measurements during the MILAGRO campaign, and very in agreement with the aged BBOA
410 from a BB experiment in a chamber study by Heringa et al. (2011). In addition, the mass
411 spectrum of OOA-BB shows more oxygenated degree, compared to mass spectrum of
412 fresh/primary BBOA from PMF analysis in the atmosphere and from laboratory open wood
413 burning (Aiken et al., 2009) and from BBOA in this study. Furthermore, the OOA-BB
414 spectrum shows rather similarity to a BBOA spectrum (dominated by oxygenated ions, i.e.
415 *m/z* 18 and *m/z* 44, and with lower fraction of *m/z* 60) observed in a wood stove with the
416 burning condition of smoldering phase (Weimer et al., 2008). This means that burn phase also
417 plays a significant role in the OOA-BB formation, and thus may influence its loadings in the
418 open BB periods. The OOA-BB spectrum in this study is also very similar to the spectrum of

419 the secondary OA produced from aged biomass smoke in a smog chamber (Grieshop et al.,
420 2009). The results suggest that OOA-BB may contain some aged/secondary BBOA, although
421 it is not precisely known whether this factor is processed OOA from BB or processed primary
422 BBOA mixed with SOA from another source in the atmosphere, as well as the burn phases.
423 OOA-BB presents a pronounced diurnal cycle with the highest concentration in the evening
424 and early morning during the harvests (Fig. 3), which is very consistent with the diurnal
425 variations of BBOA. This means that the SOA formation from open BB is rapid in short
426 timescales with the high RH and low *T* conditions in the nighttime, because volatile and
427 semi-volatile organic precursors can directly emit from field burning and it will be
428 subsequently transformed into SOA via ozonolysis (Kawamura et al., 2013) and NO_3
429 reactions in the dark. OOA-BB also shows the relatively low loadings in the daytime, due to
430 the dilution effects by enhanced mixing in the planetary boundary layer and the evaporative
431 loss of semi-volatile components along with the increase of temperature condition.
432 As shown in Fig. 4c, the OOA-BB time series strongly correlates with K^+ and Δ *m/z* 60
433 (= *m/z* 60 – 0.26% × OA, in which applied metric of background f_{60} = 0.26 % of OA will be
434 discussed in section 3.4) during the summer and autumn harvest, supporting the BB influence.
435 In addition, the sum of BBOA and OOA-BB also shows high correlation with K^+ and Δ *m/z*
436 60 for the two harvests (Fig. 5a − b). This suggests that OOA-BB represents an atmospheric
437 mixture of BBOA and OOA, which is similar to a recent HR-ToF-AMS study by Crippa et al.
438 (2013). It is interesting that OOA-BB correlates well with nitrate (r^2 = 0.30 and r^2 = 0.54), yet
439 shows lower correlation with sulfate (r^2 = 0.16 and r^2 = 0.30) for the summer and autumn
440 harvest respectively (Fig. 6). Also, the time series of OOA-BB show a similar trend with
441 chloride during the two harvest seasons (Fig. 4c). This implies an indication of the
442 semi-volatile character of OOA-BB, which is consistent with the results from a recent filed
443 study in the eastern Mediterranean (Bougiatioti et al., 2014) and some laboratory chamber

studies (Lipsky et al., 2006; Robinson et al., 2007; Yee et al., 2013). Particularly, this also means that aged biomass burning OA (OOA-BB) may be significantly mixed with nitrate in the BB plumes. Healy et al. (2013) also found a similar result in Paris using single-particle mass spectrometer (SP-AMS) and HR-ToF-AMS measurements. As shown in Figure S4, for the BB-emissions related OA (including BBOA and OOA-BB), they show a very similar wind rose pattern with high concentration from southeasterly wind during the summer harvest, and from northerly wind during the autumn harvest. This further supports that the production of OOA-BB is related to the BB plumes.

3.3 Effects of Chemical components on PM pollution

Figure 7 presents the average contributions of PM_1 species and OA components during the summer and autumn harvest, respectively. It is also compared with other sites, including megacities (Mexico City, Paris, Beijing, and Shanghai), suburban/remote areas (Crete, Jiaxing, and Pear River Delata) (Aiken et al., 2009; Crippa et al., 2013; Huang et al., 2012, 2013; Sun et al., 2012; Bougiatioti et al., 2014). Using the relative contribution of the sum of BBOA and OOA-BB to OA, the harvest season was separated into 3 time periods, i.e., low BB (L-BB, 28% and 29%) period, medium BB (M-BB, 49% and 38%) period, and high BB (H-BB, 93% and 50%) period, during the summer and autumn harvest respectively. We also include averages of some meteorological parameters (i.e. RH, *T*, WS, and WD) for the reference, and these averages are shown in Table S2.

As shown in Fig. 7, OA is important in PM pollution in the summer and autumn harvest (39% and 41%). Furthermore, the average contribution of BBOA to OA during the summer harvest (7%) is highly consistent with that in the autumn (7%), while BC shows a higher contribution during the autumn harvest (12%) than that in the summer harvest (8%). This is also corresponding to the contribution of HOA + COA, which shows a higher contribution

during the autumn harvest (28%) than that in the summer harvest (15%). The different boundary layer height and primary sources emission influences on primary pollutants (including BC, HOA and COA) may be all potential causes of such seasonal differences. On average, the total oxidized fraction of OA (including OOA and OOA-BB) accounts for more than 60% (78% for summer and 65% for autumn harvest), which indicates that regional OOA plays an important role in PM pollution in urban Nanjing during the harvest seasons. This is also corresponding to some discusses in section 3.2.4. As a comparison, OOA-BB shows a higher contribution to OA in H-BB period than that in L-BB period. The contribution of OOA-BB to OA is higher than the contribution of BBOA during the harvest seasons, even in the H-BB period. These findings indicate that "aged" BBOA plays a more significant role in PM pollution than BBOA in the BB plumes, particularly in the H-BB period. This is consistent with recent studies (Grieshop et al., 2009; Heringa et al., 2011; Lathem et al., 2013; Yee et al., 2013; Bougiatioti et al., 2014) indicating that the fresh BB emission OA can be rapidly surpassed by SOA formation within a few hours after its emission.

The secondary inorganic aerosols (including sulfate, nitrate, and ammonium) can be seen in lower fraction in the H-BB period than that in the L-BB period. However, the mass concentrations of sulfate, nitrate and ammonium are higher in the H-BB period than that in the L-BB period (Table S2) respectively. Therefore, these findings indicate that BB contributes more fraction on organics than that on the secondary inorganic aerosols in the transported pollution air masses. It is interesting that the contribution of nitrate to PM_1 is higher than the contribution of sulfate in the H-BB periods during the two harvest seasons. For example, the average contribution of nitrate to PM_1 is ~18% in the H-BB periods, which is almost twice higher than that of sulfate. However, the contribution of nitrate to PM_1 is very similar to the sulfate contribution in the L-BB periods. All of those indicate the BB are much more important source of nitrate, compared to sulfate. Similar results have also been

observed by Crippa et al. (2013), Healy et al. (2013) and Bougiatioti et al. (2014) during open BB periods.

Figure 8 presents the mass fractions of PM_1 species and OA components as a function of total PM_1 mass loadings, as well as the probability density of total PM_1 mass loadings during the summer and autumn harvest respectively. Overall, the total OA components (i.e. HOA + COA, BBOA, OOA-BB and OOA) maintained at a relatively stable level across all mass loadings during the two harvest seasons. However, OOA-BB and BBOA show a significant increase as a function of the PM_1 loadings respectively, highlighting the contribution of OOA-BB arising from BB emissions to PM pollution during the harvest seasons. During the summer harvest, the HOA + COA and BC mass fractions display a slight decrease, suggesting that local primary sources play an important in the low PM pollution period. In addition, the nitrate and sulfate contributions show a slight increase and decrease respectively, indicating additional production of nitrate mass during high PM episodes. During the autumn harvest, it also should be pointed out that the OOA mass fraction shows a slight decrease as the increasing of total PM_1 loadings, which indicates that OOA is of significant importance to the low PM pollution while at high pollution OOA-BB is more crucial. However, the contribution of HOA + COA, BC, and the secondary inorganic species to the total PM_1 loadings did not show clear PM-mass loading dependency, which indicates that the high PM pollution during the autumn harvest may be caused by the synergistic effects of all pollutants.

3.4 Estimation of BBOA directly from a tracer (Δ *m/z* 60)

The BBOA mass loadings during the harvest seasons were estimated using a simple method. As described in previous studies, the parameter f_{60}, fraction of *m/z* 60 in total OA, is considered as a marker of fresh/primary BBOA (Alfarra et al., 2007; DeCarlo et al., 2008; Aiken et al., 2009; Cubison et al., 2011). To estimate the real value of the BBOA loadings,

519 the background level of f_{60} (0.26 ± 0.1%) during little/negligible BB-influence periods
520 (non-BB periods) was determined (Fig. 9). Aiken et al. (2009) and Cubison et al. (2011) also
521 obtained a similar background level of f_{60} (0.3 ± 0.06%) for an urban city in Mexico.
522 Therefore, the levoglucosan-like species in ambient BB plumes was estimated by Δ *m/z* 60 (Δ
523 *m/z* 60 = *m/z* 60 – background value of f_{60} × OA). As shown in Fig. 5b, the strong correlations
524 (r^2 = 0.95, r^2 = 0.98, and r^2 = 0.97) between the BBOA and Δ *m/z* 60 with the similar slopes,
525 i.e., 16.3 for summer, 14.6 for autumn, and 15.1 for the total harvest seasons, were observed.
526 The OOA-BB mass loadings also show the high correlations with Δ *m/z* 60 (r^2 = 0.95 and r^2 =
527 0.97), but with very different slopes (74.8 and 64.4) during the summer and autumn harvest
528 respectively (Fig. 5b). As discussed above and by some reports (Aiken et al., 2009; DeCarlo
529 et al., 2010; Cubison et al., 2011; Crippa et al., 2013; Bougiatioti et al., 2014), this can be a
530 good evidence for explaining the OOA-BB loadings depended on the aging processes of BB
531 pollutants and its mathematically mixing of sources in the BB plumes. Aiken et al. (2009)
532 also found that BBOA strongly correlated with Δ *m/z* 60 mass loadings (r^2 = 0.91, *Slope* = 34)
533 during the BB/wood-smoke periods in Mexico City. Furthermore, Lee et al. (2010) obtained a
534 strong relationship between BBOA and *m/z* 60 mass loadings (r^2 = 0.92, *Slope* = 34.5)
535 through a wildland fuels fire experiment in the lab. Thus, we reconstructed the time series of
536 BBOA to compare the relationship between the extracted BBOA by PMF model (PMF
537 BBOA) and the estimated BBOA. As shown in Fig. 10, an excellent agreement is observed
538 between the identified and reconstructed BBOA concentrations during the total harvest
539 seasons (r^2 = 0.97). Therefore, the BBOA component during the BB periods in urban Nanjing
540 of the YRD region can be estimated with the equations of BBOA = 15.1 × (*m/z* 60 – 0.26% ×
541 OA) for the harvest seasons.
542

3.5 Evaluation of OA

Figure 11 shows the total BB-related OA (BBOA + OOA-BB) to ΔCO ratio as a function of the f_{44} during the summer and autumn harvest respectively, to investigate further the probable importance of the aging and/or mixing processes of BB plumes. The CO background is determined as 14.9 μg m^{-3} for summer harvest and 17.9 μg m^{-3} for autumn harvest, respectively, based on an average of the lowest 5% CO during two plumes (Takegawa et al., 2006). The ratio of BBOA + OOA-BB to ΔCO can remove the effect of dilution in the regional air (DeCarlo et al., 2008). As discussed in de Gouw et al. (2005), Aiken et al. (2008), Jimenez et al. (2009), and Ng et al. (2010), the f_{44} can be considered as indicator of atmospheric aging due to photochemical aging processes leading to the increasing of f_{44} in the atmosphere. Overall, the (BBOA + OOA-BB) / ΔCO ratio shows an obvious reduction with increasing of f_{44} values during the summer and autumn harvest respectively, apart from the influence of traffic and cooking-like plumes. This is likely due to a combination of rapid SOA formation from BB emissions and mixing with urban air and with higher CO content. Similar results have also been found by DeCarlo et al. (2010), from aircraft measurements during MILAGRO in Mexico City and the Central Mexican Plateau. It is interesting that the BB plumes in the summer harvest show a higher oxidation level (Δf_{44} = 0.04, within the two dashed lines of Fig. 11a − b) than that in the autumn harvest (see also Fig. 9). This might be a potential factor leading to a higher oxidation level in the mass spectra of OOA-BB in summer harvest, compared to that in the autumn harvest (Fig. 3c).

Figure 12a depicts the evolution process of OA with the f_{44} vs. f_{43} space during two harvest seasons. The BBOA and HOA + COA show similar low oxidative properties with varying f_{43}, which are located at the left-bottom of the triangular region during the summer and autumn harvest, respectively. This agrees well with the result observed by Crippa et al. (2013) in Paris. This further demonstrates that BBOA represents mainly the primary BBOA

during the harvests. As discussed above, OOA-BB could be associated to aged BBOA components with semi-volatile character in the BB plumes, which is the probably processed OOA from the BB emissions and/or emissions during specific burn phases (Weimer et al., 2008; Grieshop et al., 2009; Bougiatioti et al., 2014; Young et al., 2014). With the aging process in the atmosphere, OA clusters within a well-defined triangular region and shows more similar oxidative properties to OOA-BB and/or OOA (Fig. 12a). This implies that OOA-BB and/or BBOA might be further oxidized, and might be transformed into highly oxidized OOA. This result is also consistent with the studies of Jimenez et al. (2009) and Heringa et al. (2011).

Furthermore, the formation and transformation of primary and secondary BBOA during BB periods can be described by f_{44} vs. f_{60} plot (Cubison et al., 2011). In the f_{44} vs. f_{60} space of Fig. 12b, OA shows a trend toward higher f_{44} and lower f_{60} values with the aging/dilution of BB plumes, appearing into the low-volatility OOA (LV-OOA) range. This is very consistent with previous reports in aircraft and laboratory studies (Cubison et al., 2011) with a similar trend. In a smog chamber experiment, Grieshop et al. (2009) also found that the relative contribution at *m/z* 44 and *m/z* 60 rapidly increases and decreases, respectively during aging process, which presents the characteristics of fresh and aged BBOA.

As increasing of the f_{44} / f_{60} ratio, the mass loadings of the PM_1 and OA show decreasing trends respectively (Fig. 12c − d), suggesting that the contribution of the fresh BB plume to the PM pollution gradually decreases with the aging of evolving ambient open BB plumes. Thus, it is reasonable to believe that the fresh BB plumes significantly contribute to the ambient OA burden during the harvest seasons. Logically, a decreasing trend of the OA / ΔCO ratio is presented with increasing of the f_{44} / f_{60} ratio (Fig. 12c − d), meaning that the BB emissions might be mixing with the regional and/or urban emissions as it is aging.

3.6 Impacts of various source regions on the PM pollution

Figure 13 presents the calculated air mass 48 h BTs at 500 m arrival height above ground level at intervals of two hours (i.e. 00:00, 02:00, 04:00, …, 22:00) starting at CST using the HYSPLIT model (Draxler and Rolph, 2003) in Nanjing (118°46'N, 32°05'E). The corresponding BTs can be broadly classified into four principal clusters of air masses based on the spatial distributions during the summer and autumn harvests, respectively, i.e., northeasterly (NE) back-trajectories (BTs), easterly marine (EM) BTs, southeasterly marine (SEM) BTs, and southwesterly continental (SWC) for the summer harvest; northerly continental (NC) BTs, northeasterly marine (NEM) BTs, easterly marine (EM) BTs and southerly continental (SC) for the autumn harvest. The air masses in Nanjing in this study were mainly from the SEM BTs (accounting for 57.4% of all the BTs) during the summer harvest, while predominantly from the NC and EM BTs (at frequencies of 43.8% and 24%, respectively) during the autumn harvest (Figure 13 and Table S3).

The total PM_1 loadings are on average the highest (71.3 μg m^{-3}) for a continental-related cluster (SWS BTs), which is almost twice higher than that of the lowest (24.4 μg m^{-3}) for the marine-related cluster (EM BTs) during the summer harvest. This suggests that the long-range transported pollutants from southwestern areas can cause the high PM pollution in the YRD region during the summer harvest. Similarly, the highest average concentration of PM_1 (80.9 μg m^{-3}) associated with a continental-related cluster (SC) during the autumn harvest. Therefore, source regions are of utmost importance to the high air pollution in the YRD region during the harvest seasons.

The PM_1 chemical compositions show also significantly different fraction among the four clusters during the summer and autumn harvest respectively, which might be associated with the different source regions of air pollution. The contributions of BC, HOA + COA, and BB related OA (BBOA and OOA-BB) to PM_1 are rather high in the WC BTs, suggesting

618 that a significant impact of local primary emissions and regional agricultural open fires
619 (Figure S1) on aerosol pollution in urban Nanjing during the summer harvest. The lowest
620 PM_1 loadings are associated with the EM BTs, but with the high contribution of HOA + COA
621 during the summer harvest. This suggests that the local sources emission play an important
622 role in the relatively low PM pollution during the summer harvest. For the NE BTs, the OOA,
623 nitrate, and sulfate account the high fractions of the total PM_1 mass, suggesting that regional
624 pollution plays a key role in controlling the PM pollution. Compared with other clusters
625 during the autumn harvest, the BB related emissions (e.g. BBOA, OOA-BB, and chloride)
626 contribute the highest fractions to the PM_1 mass in air masses originated from the SC BTs,
627 indicating that BB plumes potentially contribute to the highest pollution period during the
628 summer harvest. Apart from the high contributions of nitrate and OOA, HOA + COA also
629 accounted a higher fraction to PM_1 mass in the NEM and EM BTs than that originated from
630 the others during the autumn harvest. These findings suggest that the marine-related BTs have
631 the low levels of background pollutants, which probably reflects the levels of local pollution.
632 In addition, the PM_1 components show the lowest concentrations for the NC BTs, compared
633 to the other clusters during the autumn harvest. When removing the mass concentrations of
634 BB related OA (BBOA and OOA-BB), the mean concentration of PM_1 (31.6 μg m^{-3}) for the
635 NC BTs is corresponding to a result (28.7 μg m^{-3}) for a similar cluster during a non-BB
636 period (Huang et al., 2012).
637
638 **4 Conclusions**
639 The characteristics, sources and evolution of atmospheric PM_1 species in urban Nanjing, the
640 YRD region of China were investigated using an Aerodyne ACSM during the two harvest
641 seasons, namely the summer wheat harvest (June 1 to 15, 2013) and the autumn rice harvest
642 (October 15 to 30, 2013). The PM_1 mass varies very dynamically for the two harvests,

643 ranging from 3.6 to 253.0 μg m^{-3} with a mean value of 38.16 μg m^{-3} during the summer
644 harvest, and ranged from 7.3 to 163.6 μg m^{-3} with a mean value of 46.4 μg m^{-3} during the
645 autumn harvest. The PM_1 species show a similar contribution, which on average account for
646 39% (41%) OA, 23% (20%) nitrate, 16% (14%) ammonium, 12% (11%) sulfate, 8% (13%)
647 BC, and 1% (1%) chloride during the summer (autumn) harvest. Secondary inorganic species,
648 i.e., nitrate, sulfate and ammonium, show highly similar diurnal patterns between the summer
649 and autumn harvest, meaning its similar source emissions and chemical processing. In
650 particular, OA, chloride and BC present higher concentrations in the diurnal cycles during the
651 autumn harvest than that during the summer harvest, due to larger impacts of BB and/or local
652 primary emissions during the autumn harvest.

653 PMF analysis was performed on the ACSM OA mass spectra to investigate organic
654 source apportionment during the two harvests. Four OA components were resolved including
655 two POA factors associated with traffic and cooking (HOA + COA) and biomass burning OA
656 (BBOA) emissions and two secondary factors associated with regional and highly oxidized
657 OOA and less oxidized BB-like OA (OOA-BB). Apart from HOA + COA, BBOA and
658 OOA-BB also present pronounced diurnal cycles during the harvests, with the highest
659 concentrations occurring at night due to the nighttime BB plumes over urban Nanjing. This
660 suggests that OOA-BB may be quickly oxidized a bit and condensed on the particle phase
661 during the nighttime with the high RH and low *T* conditions. The diurnal profiles of OOA are
662 similar to the sulfate with relatively flat variations, reflecting their regional pollution. OA was
663 dominated by secondary organics (OOA and OOA-BB) with the fraction more than 60% to
664 total OA mass. POA shows a lower contribution to OA during the summer (autumn) harvest,
665 traffic and cooking 15% (28%) and BB 7% (7%) emissions. The background level of f_{60} (0.26
666 ± 0.1%) was determined using the f_{44} vs. f_{60} space during the non-BB periods (in July). Thus,

667 we suggest a simpler method for estimating the BBOA loadings based on the equations of
668 BBOA = 15.1 × (*m/z* 60 – 0.26% × OA) during the harvests.

669 Overall, the (BBOA + OOA-BB) / ΔCO ratios decrease with the increasing of the f_{44}
670 with aging are observed, suggesting the combination of rapid SOA formation from BB
671 emissions and mixing with the urban pollution air. The OA mass, however, decreases with the
672 aging of BB plumes, implying that the fresh BB plumes play a key contribution to ambient
673 OA burden during the harvest seasons. Air masses trajectory analysis indicates that local
674 sources probably play an important role in the relatively low PM pollution associated with the
675 air mass originated from the marine region during the harvests. However, the high PM
676 pollution are mainly contributed by nitrate, BBOA, and OOA-BB, which is associated with
677 air masses originated from the western (summer harvest) and southern (autumn harvest)
678 areas.

679

680 *Acknowledgements*

681 This work was funded by the Natural Science Key Research of Jiangsu Province High
682 Education (11KJA170002), the Foundation Research Project of Jiangsu Province
683 (BK2012884, BK20140987), the Project Funded by the Jiangsu Province Science &
684 Technology Support Program (BE2012771), and the National Natural Science Foundation of
685 China (21407080). We are very grateful for the help and support from Dr. Douglas R.
686 Worsnop and Dr. John T. Jayne (Aerodyne Research Inc.) in the ACSM measurements. We
687 also would like to thank Dr. P. Chen (Handix LLC) and Dr. W. Li (South Coast Air Quality
688 Management District) for their constructive suggestions in improving the contents.

689

690 **References**

691 Andreae, M. O., and Merlet, P.: Emission of trace gases and aerosols from biomass burning,
692 Global Biogeochem. Cycles, 15, 955-966, 2001.
693 Alfarra, M. R., Prévôt, A. S. H., Szidat, S., Sandradewi, J., Weimer, S., Schreiber, D., Mohr,
694 M., and Baltensperger, U.: Identification of the mass spectral signature of organic
695 aerosols from wood burning emissions, Environ. Sci Technol., 41, 5770-5777, 2007.
696 Aiken, A. C., Decarlo, P. F., Kroll, J. H., Worsnop, D. R., Huffman, J. A., Docherty, K. S.,
697 Ulbrich, I. M., Mohr, C., Kimmel, J. R., Sueper, D., Sun, Y., Zhang, Q., Trimborn, A.,
698 Northway, M., Ziemann, P. J., Canagaratna, M. R., Onasch, T. B., Alfarra, M. R., Prevot,
699 A. S. H., Dommen, J., Duplissy, J., Metzger, A., Baltensperger, U., and Jimenez, J. L.:
700 O/C and OM/OC ratios of primary, secondary, and ambient organic aerosols with
701 high-resolution time-of-flight aerosol mass spectrometry, Environ. Sci. Technol., 42,
702 4478–4485, 2008.
703 Aiken, A. C., Salcedo, D., Cubison, M. J., Huffman, J. A., DeCarlo, P. F., Ulbrich, I. M.,
704 Docherty, K. S., Sueper, D., Kimmel, J. R., Worsnop, D. R., Trimborn, A., Northway, M.,
705 Stone, E. A., Schauer, J. J., Volkamer, R. M., Fortner, E., de Foy, B., Wang, J., Laskin, A.,
706 Shutthanandan, V., Zheng, J., Zhang, R., Gaffney, J., Marley, N. A., Paredes-Miranda, G.,
707 Arnott, W. P., Molina, L. T., Sosa, G., and Jimenez, J. L.: Mexico City aerosol analysis
708 during MILAGRO using high resolution aerosol mass spectrometry at the urban
709 supersite (T0) – Part 1: Fine particle composition and organic source apportionment,
710 Atmos. Chem. Phys., 9, 6633-6653, doi:10.5194/acp-9-6633-2009, 2009.
711 Aiken, A. C., de Foy, B., Wiedinmyer, C., DeCarlo, P. F., Ulbrich, I. M., Wehrli, M. N.,
712 Szidat, S., Prévôt, A. S. H., Noda, J., Wacker, L., Volkamer, R., Fortner, E., Wang, J.,
713 Laskin, A., Shutthanandan, V., Zheng, J., Zhang, R., Paredes-Miranda, G., Arnott, W. P.,
714 Molina, L. T., Sosa, G., Querol, X., and Jimenez, J. L.: Mexico city aerosol analysis

during MILAGRO using high resolution aerosol mass spectrometry at the urban supersite (T0) - Part 2: Analysis of the biomass burning contribution and the non-fossil carbon fraction, Atmos. Chem. Phys., 10, 5315-5341, doi:10.5194/acp-10-5315-2010, 2010.

Allan, J. D., Bower, K. N., Coe, H., Boudries, H., Jayne, J. T., Canagaratna, M. R., Millet, D. B., Goldstein, A. H., Quinn, P. K., Weber, R. J., W. D. R.: Submicron aerosol composition at Trinidad Head, California, during ITCT 2K2: Its relationship with gas phase volatile organic carbon and assessment of instrument performance, J. Geophys. Res., 109: D23S24, 2004.

Allan, J. D., Williams, P. I., Morgan, W. T., Martin, C. L., Flynn, M. J., Lee, J., Nemitz, E., Phillips, G. J., Gallagher, M. W., and Coe, H.: Contributions from transport, solid fuel burning and cooking to primary organic aerosols in two UK cities, Atmos. Chem. Phys., 10, 647-668, doi:10.5194/acp-10-647-2010, 2010.

Bougiatioti, A., Stavroulas, I., Kostenidou, E., Zarmpas, P., Theodosi, C., Kouvarakis, G., Canonaco, F., Prévôt, A. S. H., Nenes, A., Pandis, S. N., and Mihalopoulos, N.: Processing of biomass-burning aerosol in the eastern Mediterranean during summertime, Atmos. Chem. Phys., 14, 4793-4807, doi:10.5194/acp-14-4793-2014, 2014.

Canagaratna, M., Jayne, J., Jimenez, J. L., Allan, J. A., Alfarra, R., Zhang, Q., Onasch, T., Drewnick, F., Coe, H., Middlebrook, A., Delia, A., Williams, L., Trimborn, A., Northway, M., Kolb, C., Davidovits, P., and Worsnop, D.: Chemical and microphysical characterization of aerosols via Aerosol Mass Spectrometry, Mass Spectrom. Rev., 26, 185-222, 2007.

Canonaco, F., Crippa, M., Slowik, J. G., Baltensperger, U., and Prévôt, A. S. H.: SoFi, an IGOR-based interface for the efficient use of the generalized multilinear engine (ME-2)

739 for the source apportionment: ME-2 application to aerosol mass spectrometer data,
740 Atmos. Meas. Tech., 6, 3649-3661, doi:10.5194/amt-6-3649-2013, 2013.
741 Cheng, Y., Engling, G., He, K.-B., Duan, F.-K., Ma, Y.-L., Du, Z.-Y., Liu, J.-M., Zheng, M.,
742 and Weber, R. J.: Biomass burning contribution to Beijing aerosol, Atmos. Chem. Phys.,
743 13, 7765-7781, doi:10.5194/acp-13-7765-2013, 2013.
744 Crippa, M., DeCarlo, P. F., Slowik, J. G., Mohr, C., Heringa, M. F., Chirico, R., Poulain, L.,
745 Freutel, F., Sciare, J., Cozic, J., Di Marco, C. F., Elsasser, M., Nicolas, J. B.,
746 Marchand, N., Abidi, E., Wiedensohler, A., Drewnick, F., Schneider, J., Borrmann, S.,
747 Nemitz, E., Zimmermann, R., Jaffrezo, J.-L., Prévôt, A. S. H., and Baltensperger, U.:
748 Wintertime aerosol chemical composition and source apportionment of the organic
749 fraction in the metropolitan area of Paris, Atmos. Chem. Phys., 13, 961-981,
750 doi:10.5194/acp-13-961-2013, 2013.
751 Crippa, M., Canonaco, F., Lanz, V. A., Äijälä, M., Allan, J. D., Carbone, S., Capes, G.,
752 Ceburnis, D., Dall'Osto, M., Day, D. A., DeCarlo, P. F., Ehn, M., Eriksson, A., Freney, E.,
753 Hildebrandt Ruiz, L., Hillamo, R., Jimenez, J. L., Junninen, H., Kiendler-Scharr, A.,
754 Kortelainen, A.-M., Kulmala, M., Laaksonen, A., Mensah, A. A., Mohr, C., Nemitz, E.,
755 O'Dowd, C., Ovadnevaite, J., Pandis, S. N., Petäjä, T., Poulain, L., Saarikoski, S.,
756 Sellegri, K., Swietlicki, E., Tiitta, P., Worsnop, D. R., Baltensperger, U., and Prévôt, A. S.
757 H.: Organic aerosol components derived from 25 AMS data sets across Europe using a
758 consistent ME-2 based source apportionment approach, Atmos. Chem. Phys., 14,
759 6159-6176, doi:10.5194/acp-14-6159-2014, 2014.
760 Cubison, M. J., Ortega, A. M., Hayes, P. L., Farmer, D. K., Day, D., Lechner, M. J.,
761 Brune, W. H., Apel, E., Diskin, G. S., Fisher, J. A., Fuelberg, H. E., Hecobian, A.,
762 Knapp, D. J., Mikoviny, T., Riemer, D., Sachse, G. W., Sessions, W., Weber, R. J.,
763 Weinheimer, A. J., Wisthaler, A., and Jimenez, J. L.: Effects of aging on organic aerosol

764 from open biomass burning smoke in aircraft and laboratory studies, Atmos. Chem.
765 Phys., 11, 12049-12064, doi:10.5194/acp-11-12049-2011, 2011.
766 DeCarlo, P. F., Dunlea, E. J., Kimmel, J. R., Aiken, A. C., Sueper, D., Crounse, J.,
767 Wennberg, P. O., Emmons, L., Shinozuka, Y., Clarke, A., Zhou, J., Tomlinson, J.,
768 Collins, D. R., Knapp, D., Weinheimer, A. J., Montzka, D. D., Campos, T., and
769 Jimenez, J. L.: Fast airborne aerosol size and chemistry measurements above Mexico
770 City and Central Mexico during the MILAGRO campaign, Atmos. Chem. Phys., 8,
771 4027-4048, doi:10.5194/acp-8-4027-2008, 2008.
772 DeCarlo, P. F., Ulbrich, I. M., Crounse, J., de Foy, B., Dunlea, E. J., Aiken, A. C., Knapp, D.,
773 Weinheimer, A. J., Campos, T., Wennberg, P. O., and Jimenez, J. L.: Investigation of the
774 sources and processing of organic aerosol over the Central Mexican Plateau from
775 aircraft measurements during MILAGRO, Atmos. Chem. Phys., 10, 5257-5280,
776 doi:10.5194/acp-10-5257-2010, 2010.
777 de Gouw, J. A., Middlebrook, A. M., Warneke, C., Goldan, P. D., Kuster, W. C., Roberts, J.
778 M., Fehsenfeld, F. C., Worsnop, D. R., Canagaratna, M. R., Pszenny, A. A. P., Keene, W.
779 C., Marchewka, M., Bertman, S. B., and Bates, T. S.: Budget of organic carbon in a
780 polluted atmosphere: Results from the New England Air Quality Study in 2002, J.
781 Geophys. Res. Atmos., 110, D16305, 2005.
782 Ding, A. J., Fu, C. B., Yang, X. Q., Sun, J. N., Petäjä, T., Kerminen, V.-M., Wang, T., Xie, Y.,
783 Herrmann, E., Zheng, L. F., Nie, W., Liu, Q., Wei, X. L., and Kulmala, M.: Intense
784 atmospheric pollution modifies weather: a case of mixed biomass burning with fossil
785 fuel combustion pollution in eastern China, Atmos. Chem. Phys., 13, 10545-10554,
786 doi:10.5194/acp-13-10545-2013, 2013.

787 Draxler, R. R., Rolph, G. D.: HYSPLIT (HYbrid Single-Particle Lagrangian Integrated
788 Trajectory) Model Access via NOAA ARL READY Website. NOAA Air Resources
789 Laboratory, Silver Spring, MD. http://www.arl.noaa.gov/ready/hysplit4.html, 2003.
790 Du, H. H., Kong, L.D., Cheng, T.T., Chen, J.M., Du, J.F., Li, L., Xia, X.G., Leng, C.P., Huang,
791 G. H.: Insights into summertime haze pollution events over Shanghai based on online
792 water-soluble ionic composition of aerosols, Atmos. Environ., 45, 5131-5137, 2011.
793 Gilardoni, S., Liu, S., Takahama, S., Russell, L. M., Allan, J. D., Steinbrecher, R., Jimenez, J.
794 L., De Carlo, P. F., Dunlea, E. J., and Baumgardner, D.: Characterization of organic
795 ambient aerosol during MIRAGE 2006 on three platforms, Atmos. Chem. Phys., 9,
796 5417-5432, doi:10.5194/acp-9-5417-2009, 2009.
797 Grieshop, A. P., Donahue, N. M., and Robinson, A. L.: Laboratory investigation of
798 photochemical oxidation of organic aerosol from wood fires 2: analysis of aerosol mass
799 spectrometer data, Atmos. Chem. Phys., 9, 2227-2240, doi:10.5194/acp-9-2227-2009,
800 2009.
801 He, L.-Y., Lin, Y., Huang, X.-F., Guo, S., Xue, L., Su, Q., Hu, M., Luan, S.-J., and
802 Zhang, Y.-H.: Characterization of high-resolution aerosol mass spectra of primary
803 organic aerosol emissions from Chinese cooking and biomass burning, Atmos. Chem.
804 Phys., 10, 11535-11543, doi:10.5194/acp-10-11535-2010, 2010.
805 Healy, R. M., Sciare, J., Poulain, L., Crippa, M., Wiedensohler, A., Prévôt, A. S. H.,
806 Baltensperger, U., Sarda-Estève, R., McGuire, M. L., Jeong, C.-H., McGillicuddy, E.,
807 O'Connor, I. P., Sodeau, J. R., Evans, G. J., and Wenger, J. C.: Quantitative
808 determination of carbonaceous particle mixing state in Paris using single-particle mass
809 spectrometer and aerosol mass spectrometer measurements, Atmos. Chem. Phys., 13,
810 9479-9496, doi:10.5194/acp-13-9479-2013, 2013.

Heringa, M. F., DeCarlo, P. F., Chirico, R., Tritscher, T., Dommen, J., Weingartner, E., Richter, R., Wehrle, G., Prévôt, A. S. H., and Baltensperger, U.: Investigations of primary and secondary particulate matter of different wood combustion appliances with a high-resolution time-of-flight aerosol mass spectrometer, Atmos. Chem. Phys., 11, 5945-5957, doi:10.5194/acp-11-5945-2011, 2011.

Hu, W. W., Hu, M., Yuan, B., Jimenez, J. L., Tang, Q., Peng, J. F., Hu, W., Shao, M., Wang, M., Zeng, L. M., Wu, Y. S., Gong, Z. H., Huang, X. F., and He, L. Y.: Insights on organic aerosol aging and the influence of coal combustion at a regional receptor site of central eastern China, Atmos. Chem. Phys., 13, 10095-10112, doi:10.5194/acp-13-10095-2013, 2013.

Huang, X.-F., He, L.-Y., Hu, M., Canagaratna, M. R., Sun, Y., Zhang, Q., Zhu, T., Xue, L., Zeng, L.-W., Liu, X.-G., Zhang, Y.-H., Jayne, J. T., Ng, N. L., and Worsnop, D. R.: Highly time-resolved chemical characterization of atmospheric submicron particles during 2008 Beijing Olympic Games using an Aerodyne High-Resolution Aerosol Mass Spectrometer, Atmos. Chem. Phys., 10, 8933-8945, doi:10.5194/acp-10-8933-2010, 2010.

Huang, X.-F., He, L.-Y., Hu, M., Canagaratna, M. R., Kroll, J. H., Ng, N. L., Zhang, Y.-H., Lin, Y., Xue, L., Sun, T.-L., Liu, X.-G., Shao, M., Jayne, J. T., and Worsnop, D. R.: Characterization of submicron aerosols at a rural site in Pearl River Delta of China using an Aerodyne High-Resolution Aerosol Mass Spectrometer, Atmos. Chem. Phys., 11, 1865-1877, doi:10.5194/acp-11-1865-2011, 2011.

Huang, X.-F., He, L.-Y., Xue, L., Sun, T.-L., Zeng, L.-W., Gong, Z.-H., Hu, M., and Zhu, T.: Highly time-resolved chemical characterization of atmospheric fine particles during 2010 Shanghai World Expo, Atmos. Chem. Phys., 12, 4897-4907, doi:10.5194/acp-12-4897-2012, 2012.

836 Huang, X.-F., Xue, L., Tian, D.-X., Shao, W.-W., Sun, T.-L., Gong, Z.-H., Ju, W.-W., Jiang,
837 B., Hu, M., and He, L.-Y.: Highly time-resolved carbonaceous aerosol characterization
838 in Yangtze River Delta of China: Composition, mixing state and secondary formation,
839 Atmos. Environ., 64, 200-207, 2013.
840 Huffman, J. A., Docherty, K. S., Aiken, A. C., Cubison, M. J., Ulbrich, I. M., DeCarlo, P. F.,
841 Sueper, D., Jayne, J. T., Worsnop, D. R., Ziemann, P. J., and Jimenez, J. L.:
842 Chemically-resolved aerosol volatility measurements from two megacity field studies,
843 Atmos. Chem. Phys., 9, 7161-7182, doi:10.5194/acp-9-7161-2009, 2009.
844 Jimenez, J. L., Canagaratna, M. R., Donahue, N. M., Prévôt, A. S. H., Zhang, Q., Kroll, J. H.,
845 DeCarlo, P. F., Allan, J. D., Coe, H., Ng, N. L., Aiken, A. C., Docherty, K. S., Ulbrich, I.
846 M., Grieshop, A. P., Robinson, A. L., Duplissy, J., Smith, J. D., Wilson, K. R., Lanz, V.
847 A., Hueglin, C., Sun, Y. L., Tian, J., Laaksonen, A., Raatikainen, T., Rautiainen, J.,
848 Vaattovaara, P., Ehn, M., Kulmala, M., Tomlinson, J. M., Collins, D. R., Cubison, M. J.,
849 E, Dunlea, J., Huffman, J. A., Onasch, T. B., Alfarra, M. R., Williams, P. I., Bower, K.,
850 Kondo, Y., Schneider, J., Drewnick, F., Borrmann, S., Weimer, S., Demerjian, K.,
851 Salcedo, D., Cottrell, L., Griffin, R., Takami, A., Miyoshi, T., Hatakeyama, S., Shimono,
852 A., Sun, J. Y., Zhang, Y. M., Dzepina, K., Kimmel, J. R., Sueper, D., Jayne, J. T.,
853 Herndon, S. C., Trimborn, A. M., Williams, L. R., Wood, E. C., Middlebrook, A. M.,
854 Kolb, C. E., Baltensperger, U., and Worsnop, D. R.: Evolution of organic aerosols in the
855 atmosphere, Science, 326, 1525-1529, 2009.
856 Justice, C. O., Giglio, L., Korontzi, S., Owens, J., Morisette, J.T., Roy, D., Descloitres, J.,
857 Alleaume, S., Petitcolin, F., Kaufman, Y.: The MODIS fire products, Remote Sens.
858 Environ., 83, 244-262, 2002.
859 Kaufman, Y. J., Tanre, D., and Boucher, O.: A satellite view of aerosols in the climate system,
860 Nature, 419: 215-23, 2002.

Kaufman, Y. J., Ichoku, C., Giglio, L., Korontzi, S., Chu, D. A., Hao, W. M., Li R. R., Justice, C. O.: Fire and smoke observed from the Earth Observing System MODIS instrument-products, validation, and operational use, Int. J. Remote Sensing, 24, 1765-781, 2003.

Kawamura, K., Tachibana, E., Okuzawa, K., Aggarwal, S. G., Kanaya, Y., and Wang, Z. F.: High abundances of water-soluble dicarboxylic acids, ketocarboxylic acids and α-dicarbonyls in the mountaintop aerosols over the North China Plain during wheat burning season, Atmos. Chem. Phys., 13, 8285-8302, doi:10.5194/acp-13-8285-2013, 2013.

Lanz, V. A., Alfarra, M. R., Baltensperger, U., Buchmann, B., Hueglin, C., and Prévôt, A. S. H.: Source apportionment of submicron organic aerosols at an urban site by factor analytical modelling of aerosol mass spectra, Atmos. Chem. Phys., 7, 1503-1522, doi:10.5194/acp-7-1503-2007, 2007.

Lee, T., Sullivan, A. P., Mack, L., Jimenez, J. L., Kreidenweis, S. M., Onasch, T. B., Worsnop, D. R., Malm, W., Wold, C. E., Hao, W. M., and Collett, J. L.: Chemical Smoke Marker Emissions During Flaming and Smoldering Phases of Laboratory Open Burning of Wildland Fuels, Aerosol Sci. Tech., 44, 1-5, 2010.

Lipsky, E. M. and Robinson, A. L.: Effects of dilution on fine particle mass and partitioning of semivolatile organics in diesel exhaust and wood smoke, Environ. Sci. Technol., 40, 155–162, 2006.

Li, X. H., Wang, S. X., Duan, L., Hao, J. M., Li, Y. S., and Yang, L.: Particulate and Trace Gas Emissions from Open Burning of Wheat Straw and Corn Stover in China, Environ. Sci. Technol., 41 (17): 6052-6058, 2007.

Liu, D., Allan, J., Corris, B., Flynn, M., Andrews, E., Ogren, J., Beswick, K., Bower, K., Burgess, R., Choularton, T., Dorsey, J., Morgan, W., Williams, P. I., and Coe, H.:

886 Carbonaceous aerosols contributed by traffic and solid fuel burning at a polluted rural
887 site in Northwestern England, Atmos. Chem. Phys., 11, 1603-1619,
888 doi:10.5194/acp-11-1603-2011, 2011.
889 Liu, D., Allan, J. D., Young, D. E., Coe, H., Beddows, D., Fleming, Z. L., Flynn, M. J.,
890 Gallagher, M. W., Harrison, R. M., Lee, J., Prevot, A. S. H., Taylor, J. W., Yin, J.,
891 Williams, P. I., and Zotter, P.: Size distribution, mixing state and source apportionments
892 of black carbon aerosols in London during winter time, Atmos. Chem. Phys. Discuss.,
893 14, 16291-16349, doi:10.5194/acpd-14-16291-2014, 2014.
894 Maenhaut, W., Vermeylen, R., Claeys, M., Vercauteren, J., Matheeussen, C., Roekens, E.:
895 Assessment of the contribution from wood burning to the PM_{10} aerosol in Flanders,
896 Belgium, Sci. Total Environ., 437, 226-236, 2012.
897 Middlebrook, A. M., Bahreini, R., Jimenez, J. L., and Canagaratna, M. R.: Evaluation of
898 Composition-Dependent Collection Efficiencies for the Aerodyne Aerosol Mass
899 Spectrometer using Field Data, Aerosol Sci. Tech., 46, 258-271, 2011.
900 Mohr, C., Huffman, J. A., Cubison, M. J., Aiken, A. C., Docherty, K. S., Kimmel, J. R.,
901 Ulbrich, I. M., Hannigan, M., and Jimenez, J. L.: Characterization of primary organic
902 aerosol emissions from meat cooking, trash burning, and motor vehicles with
903 High-Resolution Aerosol Mass Spectrometry and comparison with ambient and chamber
904 observations, Environ. Sci. Technol., 43, 2443-2449, 2009.
905 Mohr, C., DeCarlo, P. F., Heringa, M. F., Chirico, R., Slowik, J. G., Richter, R., Reche, C.,
906 Alastuey, A., Querol, X., Seco, R., Peñuelas, J., Jiménez, J. L., Crippa, M.,
907 Zimmermann, R., Baltensperger, U., and Prévôt, A. S. H.: Identification and
908 quantification of organic aerosol from cooking and other sources in Barcelona using
909 aerosol mass spectrometer data, Atmos. Chem. Phys., 12, 1649-1665,
910 doi:10.5194/acp-12-1649-2012, 2012.

911 Ng, N. L., Canagaratna, M. R., Zhang, Q., Jimenez, J. L., Tian, J., Ulbrich, I. M., Kroll, J. H.,
912 Docherty, K. S., Chhabra, P. S., Bahreini, R., Murphy, S. M., Seinfeld, J. H.,
913 Hildebrandt, L., Donahue, N. M., DeCarlo, P. F., Lanz, V. A., Prévôt, A. S. H., Dinar, E.,
914 Rudich, Y., and Worsnop, D. R.: Organic aerosol components observed in Northern
915 Hemispheric datasets from Aerosol Mass Spectrometry, Atmos. Chem. Phys., 10,
916 4625-4641, doi:10.5194/acp-10-4625-2010, 2010.
917 Ng, N. L., Herndon, S. C., Trimborn, A., Canagaratna, M. R., Croteau, P. L., Onasch, T. B.,
918 Sueper, D., Worsnop, D. R., Zhang, Q., Sun, Y. L., and Jayne, J. T.: An Aerosol
919 Chemical Speciation Monitor (ACSM) for Routine Monitoring of the Composition and
920 Mass Concentrations of Ambient Aerosol, Aerosol Sci. Technol., 45: 7, 770 -784, 2011a.
921 Ng, N. L., Canagaratna, M. R., Jimenez, J. L., Chhabra, P. S., Seinfeld, J. H., and
922 Worsnop, D. R.: Changes in organic aerosol composition with aging inferred from
923 aerosol mass spectra, Atmos. Chem. Phys., 11, 6465-6474,
924 doi:10.5194/acp-11-6465-2011, 2011b.
925 Ng, N. L., Canagaratna, M. R., Jimenez, J. L., Zhang, Q., Ulbrich, I. M., and Worsnop, D. R.:
926 Real-Time Methods for Estimating Organic Component Mass Concentrations from
927 Aerosol Mass Spectrometer Data, Environ. Sci. Technol., 45, 910-916, 2011c.
928 Paatero, P.: Least squares formulation of robust non-negative factor analysis, Chemom. Intell.
929 Lab. Syst., 37, 23-35, 1997.
930 Paatero, P.: The multilinear engine – A table-driven, least squares program for solving
931 multilinear problems, including the n-way parallel factor analysis model, J. Comput.
932 Graph. Stat., 8, 854–888, 1999.
933 Reche, C., Viana, M., Amato, F., Alastuey, A., Moreno, T., Hillamo, R., Teinila, K., Saarnio,
934 K., Seco, R., Penuelas, J., Mohr, C., Prévôt, A. S. H., and Querol, X,.: Biomass burning

contributions to urban aerosols in a coastal Mediterranean City, Sci. Total Environ., 427, 175-190, 2012.

Sandradewi, J., Prevot, A. S. H., Szidat, S., Perron, N., Alfarra, M. R., Lanz, V. A., Weingartner, E., and Baltensperger, U.: Using aerosol light absorption measurements for the quantitative determination of wood burning and traffic emission contributions to particulate matter, Environ. Sci. Technol., 42, 3316–3323, 2008.

Sun, J. Y., Zhang, Q., Canagaratna, M. R., Zhang, Y. M., Ng, N. L., Sun, Y. L., Jayne, J. T., Zhang, X. C., Zhang, X. Y., and Worsnop, D. R.: Highly time-and size-resolved characterization of submicron aerosol particles in Beijing using an Aerodyne Aerosol Mass Spectrometer, Atmos. Environ., 44, 131-140, 2010.

Sun, Y.-L., Zhang, Q., Schwab, J. J., Demerjian, K. L., Chen, W.-N., Bae, M.-S., Hung, H.-M., Hogrefe, O., Frank, B., Rattigan, O. V., and Lin, Y.-C.: Characterization of the sources and processes of organic and inorganic aerosols in New York city with a high-resolution time-of-flight aerosol mass apectrometer, Atmos. Chem. Phys., 11, 1581-1602, doi:10.5194/acp-11-1581-2011, 2011a.

Sun, Y. L., Zhang, Q., Schwab, J. J., Chen, W. N., Bae, M. S., Lin, Y. C., Hung, H. M., and Demerjian, K. L.: A case study of aerosol processing and evolution in summer in New York City, Atmos. Chem. Phys., 11, 12737-12750, doi:10.5194/acp-11-12737-2011, 2011b.

Sun, Y. L., Wang, Z. F., Dong, H. B., Yang, T., Li, J., Pan, X. L., Chen, P., and Jayne, J. T.: Characterization of summer organic and inorganic aerosols in Beijing, China with an Aerosol Chemical Speciation Monitor, Atmos. Environ., 51, 250-259, 2012.

Sun, Y. L., Wang, Z. F., Fu, P. Q., Yang, T., Jiang, Q., Dong, H. B., Li, J., and Jia, J. J.: Aerosol composition, sources and processes during wintertime in Beijing, China, Atmos. Chem. Phys., 13, 4577-4592, doi:10.5194/acp-13-4577-2013, 2013.

960 Takegawa, N., Miyakawa, T., Kondo, Y., Jimenez, J. L., Zhang, Q., Worsnop, D. R., and
961 Fukuda, M.: Seasonal and diurnal variations of submicron organic aerosol in Tokyo
962 observed using the Aerodyne aerosol mass spectrometer, J. Geophys. Res., 111, D11206,
963 2006.
964 Ulbrich, I. M., Canagaratna, M. R., Zhang, Q., Worsnop, D. R., and Jimenez, J. L.:
965 Interpretation of organic components from Positive Matrix Factorization of aerosol mass
966 spectrometric data, Atmos. Chem. Phys., 9, 2891–2918, doi:10.5194/acp-9-2891-2009,
967 2009.
968 Wang, G. H., Kawamura, K., Xie, M. J., Hu, S. Y., Cao, J. J., An, Z. H., Waston J. G., and
969 Chow, J. C.: Organic Molecular Compositions and Size Distributions of Chinese
970 Summer and Autumn Aerosols from Nanjing: Characteristic Haze Event Caused by
971 Wheat Straw Burning, Environ. Sci. Technol., 43 (17): 6493-6499, 2009a.
972 Wang, Y. Q., Zhang, X. Y., and Draxler, R. R.: TrajStat: GIS-based software that uses various
973 trajectory statistical analysis methods to identify potential sources from long-term air
974 pollution measurement data, Environ. Modell. Softw., 24: 938-939, 2009b.
975 Watson, J. G.: Visibility: Science and regulation, J. Air Waste Manage. Assoc., 52, 628-713,
976 2002.
977 Weimer, S., Alfarra, M. R., Schreiber, D., Mohr, M., Prévôt, A. S. H., and Baltensperger, U.:
978 Organic aerosol mass spectral signatures from wood-burning emissions: Influence of
979 burning conditions and wood type, J. Geophys. Res., 113, D10304,
980 doi:10.1029/2007JD009309, 2008.
981 Yee, L. D., Kautzman, K. E., Loza, C. L., Schilling, K. A., Coggon, M. M., Chhabra, P. S.,
982 Chan, M. N., Chan, A. W. H., Hersey, S. P., Crounse, J. D., Wennberg, P. O., Flagan, R.
983 C., and Seinfeld, J. H.: Secondary organic aerosol formation from biomass burning

intermediates: phenol and methoxyphenols, Atmos. Chem. Phys., 13, 8019-8043, doi:10.5194/acp-13-8019-2013, 2013.

Zhang, H., Ye, X., Cheng, T., Chen, J., Yang, X., Wang, L., Zhang, R.: A laboratory study of agricultural crop residue combustion in China: Emission factors and emission inventory, Atmos. Environ., 42, 8432-8441, 2008.

Zhang, Q., Worsnop, D. R., Canagaratna, M. R., and Jimenez, J. L.: Hydrocarbon-like and oxygenated organic aerosols in Pittsburgh: insights into sources and processes of organic aerosols, Atmos. Chem. Phys., 5, 3289-3311, doi:10.5194/acp-5-3289-2005, 2005a.

Zhang, Q., Alfarra, M.R. Worsnop, D., Allan, J. D., Coe, H., Cangaratna, M. R., Jimenez, J. L.: Deconvolution and Quantification of Hydrocarbon-like and Oxygenated Organic Aerosols Based on Aerosol Mass Spectrometry, Environ. Sci. Technol., 39, 4938-4952, 2005b.

Zhang, Q., Jimenez, J. L., Canagaratna, M. R., Allan, J. D, Coe, H., Ulbrich, I. M., Alfarra, M. R., Takami, A., Middlebrook, A. M., Sun, Y. L., Dzepina, K., Dunlea, E., Docherty, K., DeCarlo, P, F., Salcedo, D., Onasch, T., Jayne, J. T., Miyoshi, T., Shimono, A., Hatakeyama, S., Takegawa, N., Kondo, Y., Schneider, J., Drewnick, F., Borrmann, S., Weimer, S., Demerjian, K., Williams, P., Bower, K., Bahreini, R., Cottrell, L., Griffin, R. J., Rautiainen, J., Sun, J. Y., Zhang, Y. M., Worsnop, D. R.: Ubiquity and dominance of oxygenated species in organic aerosols in anthropogenically-influenced Northern Hemisphere midlatitudes, Geophys. Res. Lett., 34(13): L13801, 2007.

Zhang, Q., Jimenez, J. L., Canagaratna, M. R., Ulbrich, I. M., Ng, N. L., Worsnop, D. R., Sun, Y. L.: Understanding atmospheric organic aerosols via factor analysis of aerosol mass spectrometry: a review, Anal. Bioanal. Chem., 401:3045-3067, 2011.

1008 Table 1

1009 Mean mass concentration of PM_1 (NR-PM_1 + BC) (μg m^{-3}) and standard deviation (S.D.) during the

1010 harvest seasons.

Species	Summer harvest		Autumn harvest	
	Mean	S.D.	Mean	S.D.
NO_3	9.0	7.1	9.2	6.2
SO_4	5.0	2.4	4.7	2.5
NH_4	7.0	3.5	6.4	3.5
Chl	0.4	0.9	0.7	0.8
OA	15.4	12.8	22.3	17.5
BC	3.2	2.2	6.0	3.8
PM_1	38.5	24.3	46.4	27.0
HOA + COA	2.2	2.4	5.7	7.6
BBOA	1.1	1.0	1.5	1.6
OOA-BB	4.1	4.6	6.5	7.3
OOA	7.1	3.6	6.6	3.2

1011

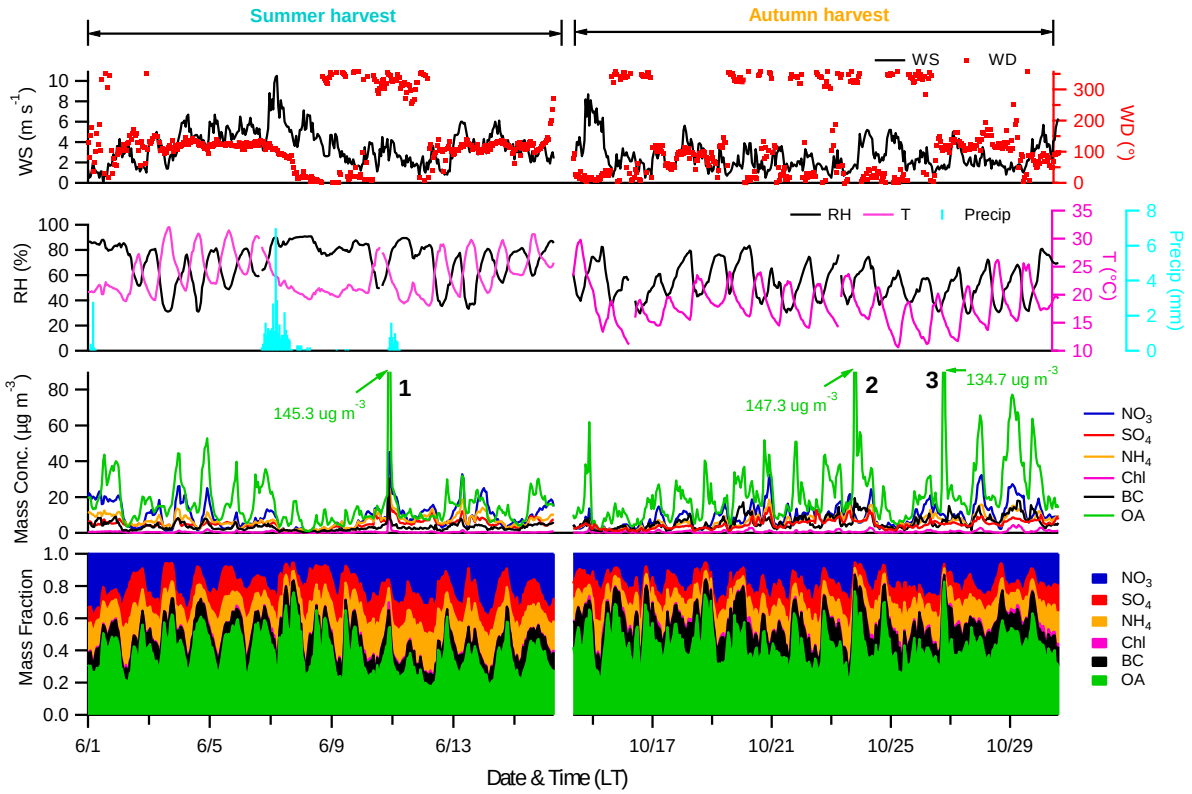

Fig. 1. Time series of **(a)** wind speed (WS) and wind direction (WD); **(b)** relative humidity (RH), temperature (*T*) and precipitation (Precip); **(c)** submicron aerosol species, i.e., organic aerosol (OA), ammonium (NH_4), nitrate (NO_3), sulfate (SO_4), chloride (Chl) and black carbon (BC); and **(d)** mass fraction during the harvest seasons. Three case events are marked and discussed in the text.

1017

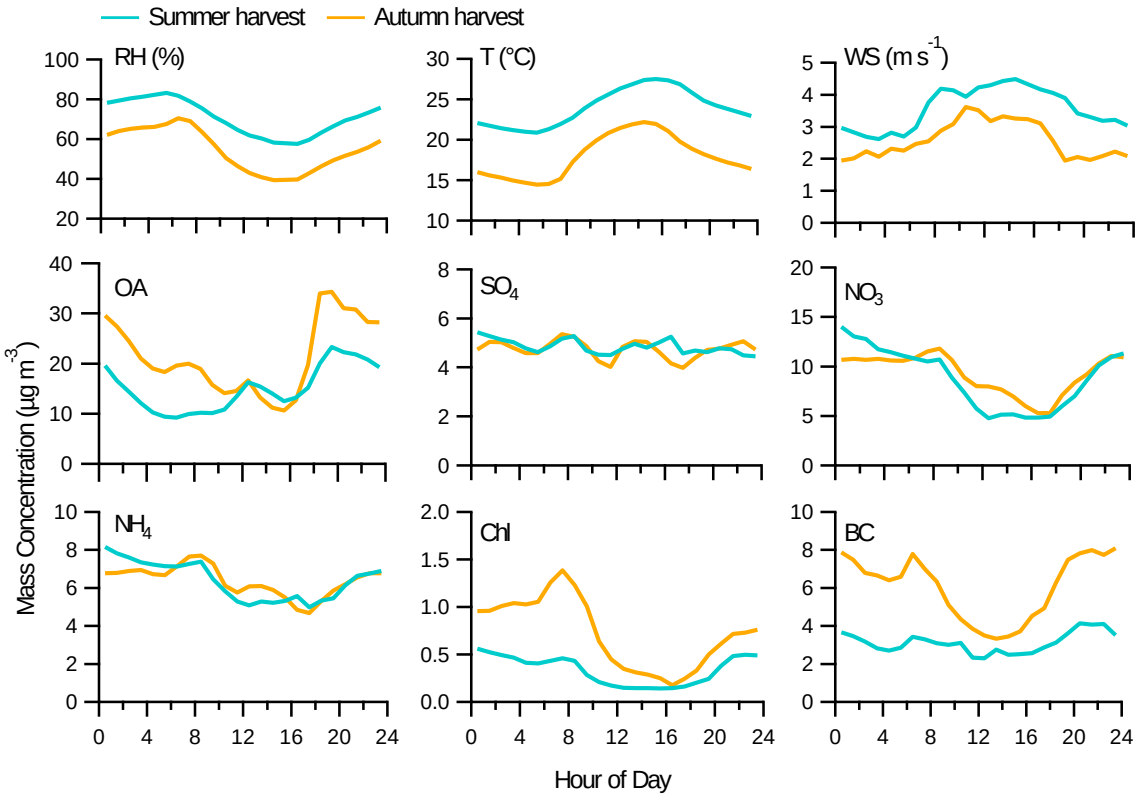

1018

1019 **Fig. 2.** Diurnal variation patterns of meteorological factors (i.e. RH, *T*, and WS), PM_1 species including

1020 organic aerosol (OA), nitrate (NO_3), sulfate (SO_4), ammonium (NH_4), chloride (Chl), and black carbon

1021 (BC) during the harvest seasons.

1022

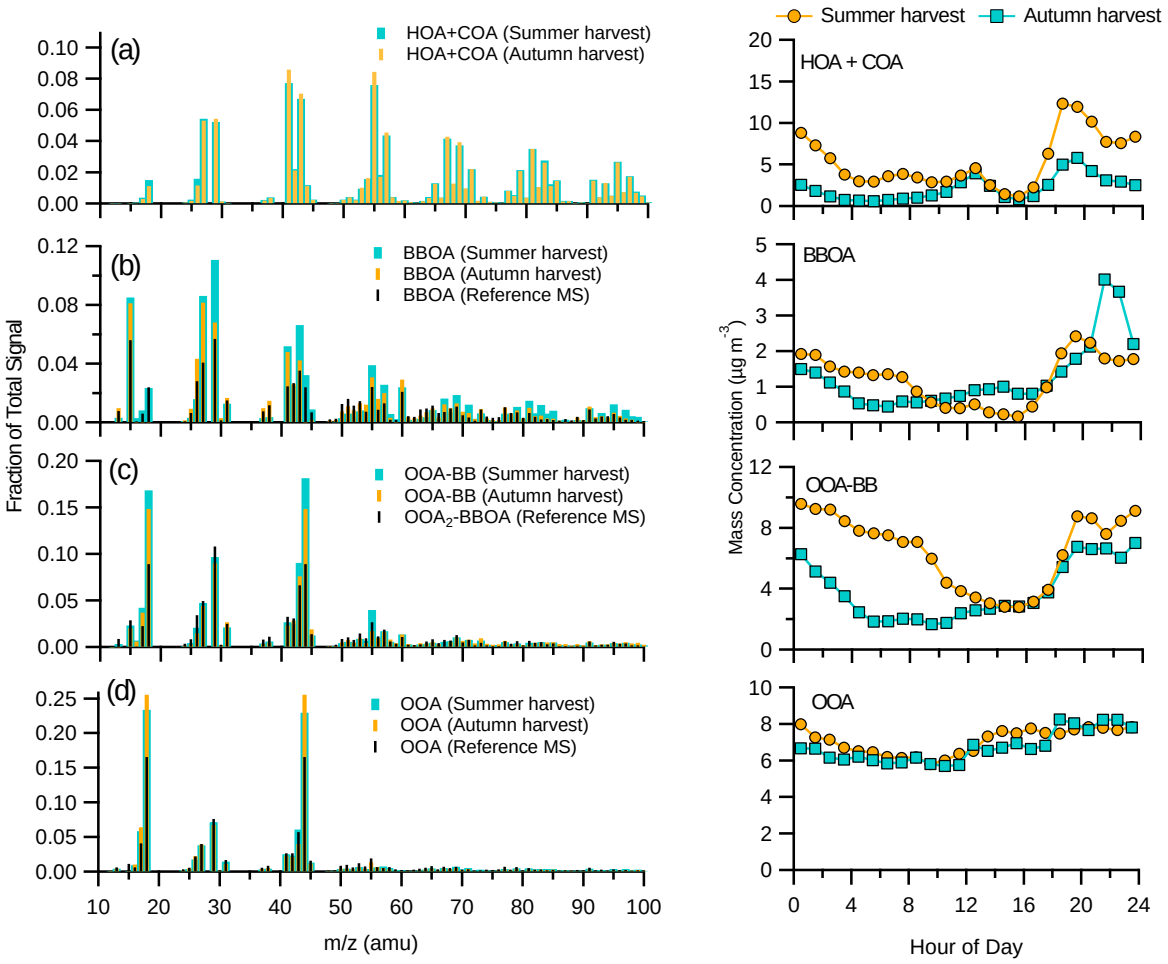

Fig. 3. Mass spectra profiles (left) and diurnal variations (right) of four OA factors, i.e., hydrocarbon-like and cooking-emission related OA (HOA + COA), fresh biomass burning (BB) OA (BBOA), oxygenated BB-influenced OA (OOA-BB), and highly oxygenated OA (OOA). Note that: reference mass spectra (MS) is from the results by Crippa et al. (2013), and OOA_2-BBOA is represented for oxygenated BBOA components.

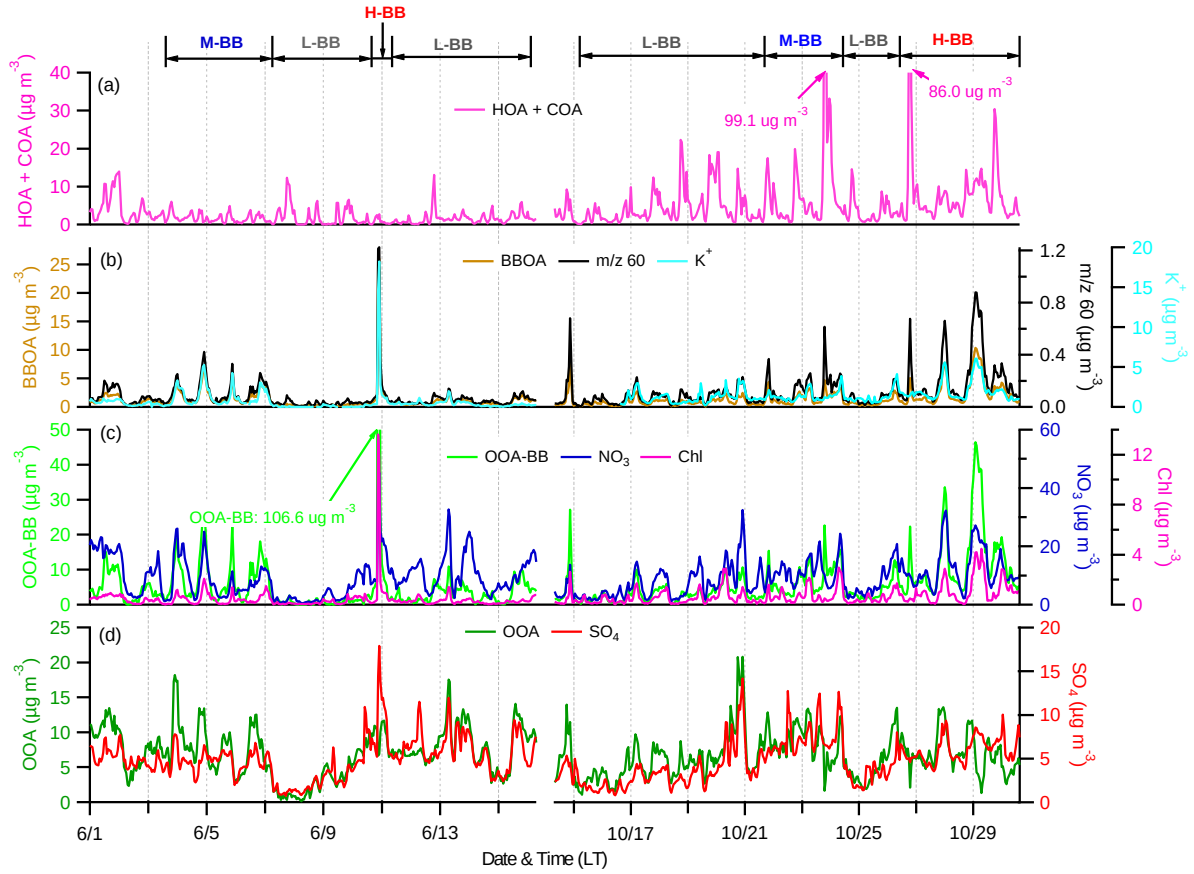

Fig. 4. Time series of OA factors (left) and relevant tracer species (right): **(a)** HOA + COA; **(b)** BBOA and a surrogate of levoglucosan (*m/z* 60) and potassium ion (K^+); **(c)** OOA-BB, nitrate and chloride; **(d)** OOA and SO_4. Note that different BBOA mass concentrations for the low biomass burning period (L-BB), medium biomass burning period (M-BB), and high biomass burning period (H-BB). Note that the H-BB in the summer harvest is corresponding to the case 1 in Fig. 1c.

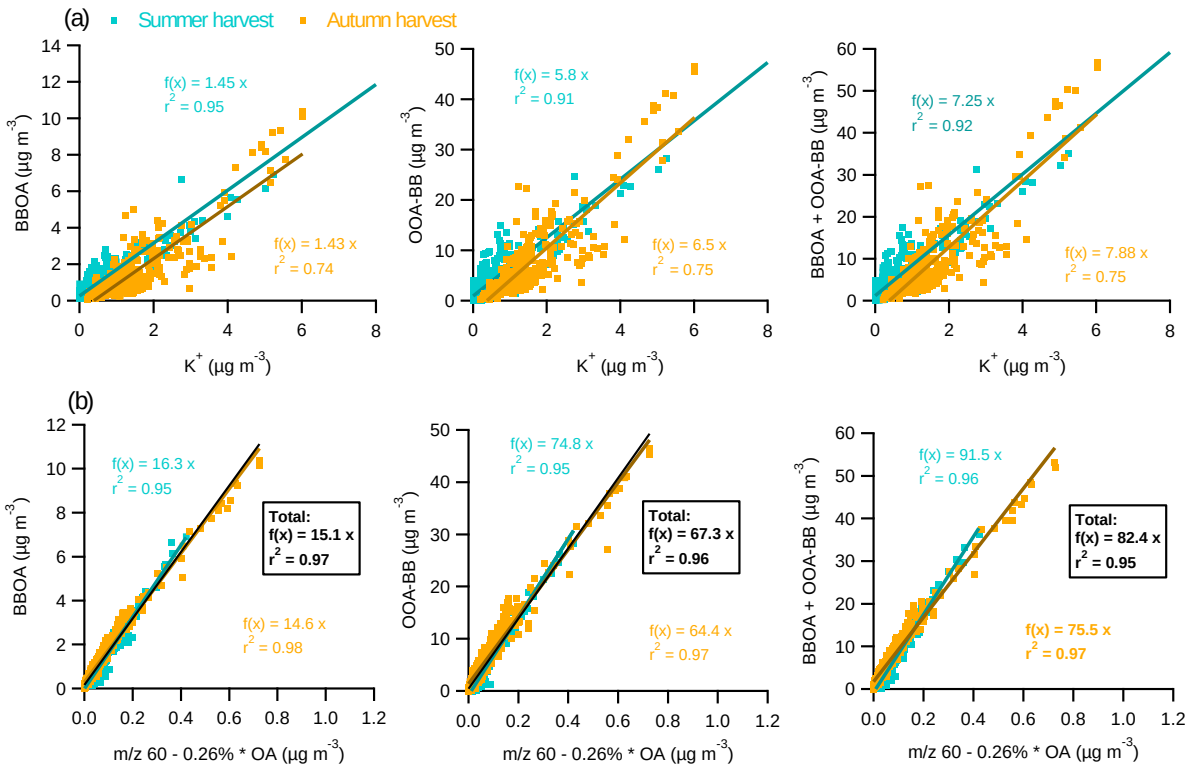

Fig. 5. Comparison of biomass burning-related PMF factors (BBOA and OOA-BB) and biomass related species: **(a)** K^+; and **(b)** the ACSM *m/z* 60 minus 0.26% × OA (applied metric of background f_{60} = 0.26 % of OA will be discussed in section 3.4) during the summer and autumn harvest respectively.

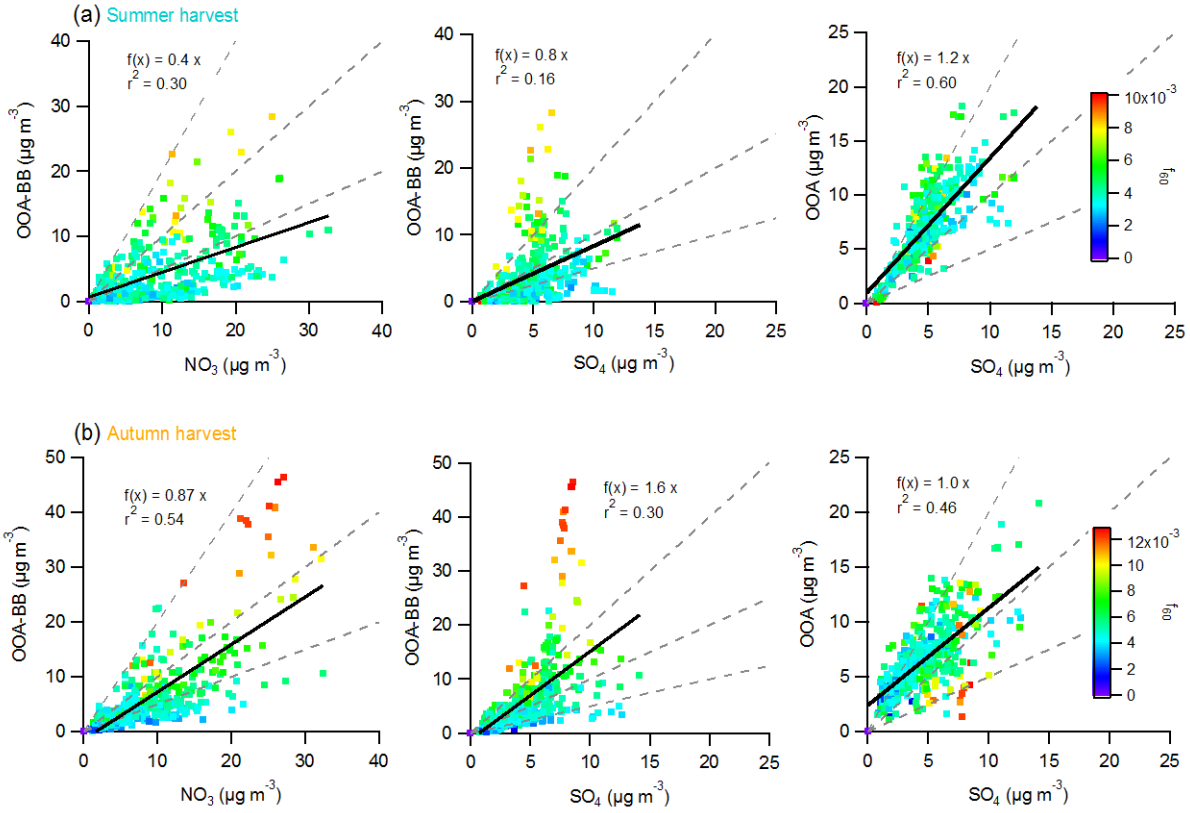

Fig. 6. Comparison of two kinds of oxygenated OA (OOA-BB and OOA) and two kinds of secondary inorganic species, i.e., nitrate (NO_3) and sulfate (SO_4), during the harvest seasons. Colored by the f_{60} as a biomass-burning marker. The three dashed lines in the plot refer to 2 : 1, 1 : 1, and 1 : 2 lines, respectively.

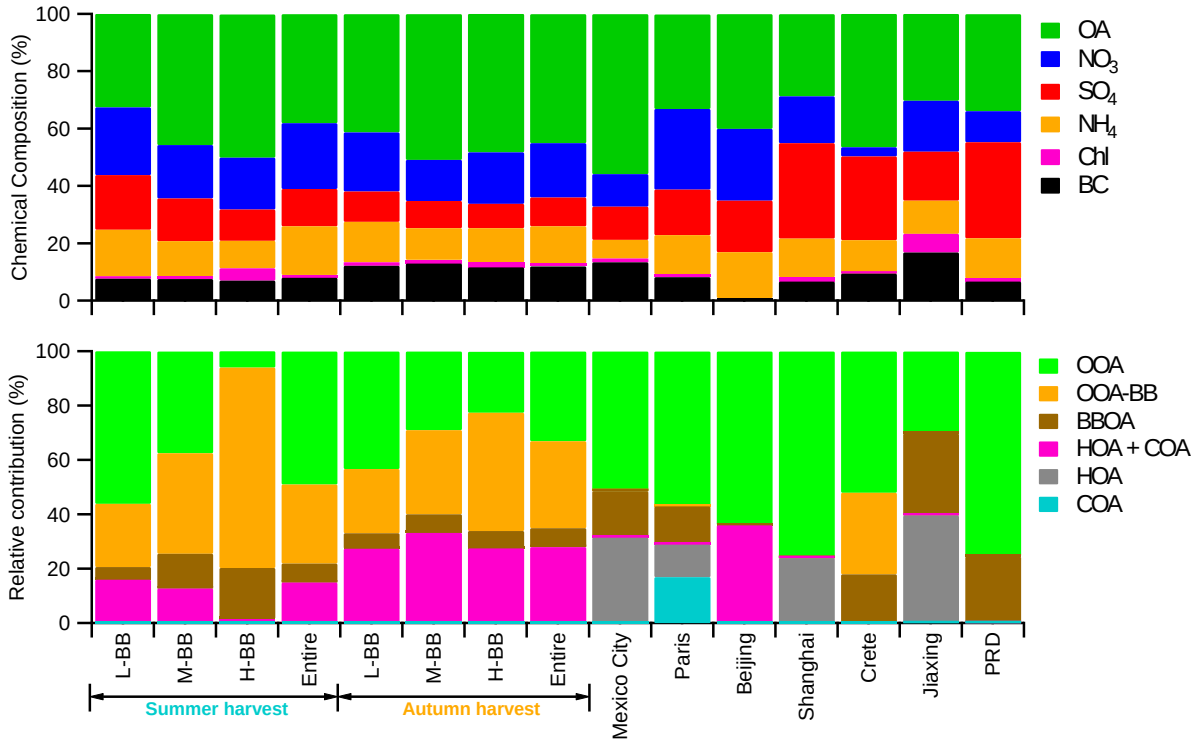

1047

1048 **Fig. 7.** Averagely relative contributions of PM_1 species and OA components for L-BB, M-BB, H-BB, and
1049 entire period during the harvest seasons and other sites including mega-cities cities (Mexico city, Paris,
1050 Beijing and Shanghai), suburban area (Jiaxing), remote background site (Crete), and PRD (Pear River
1051 Delta, China). Note that OOA in this plot includes OOA_2-BBOA in Paris.

1052

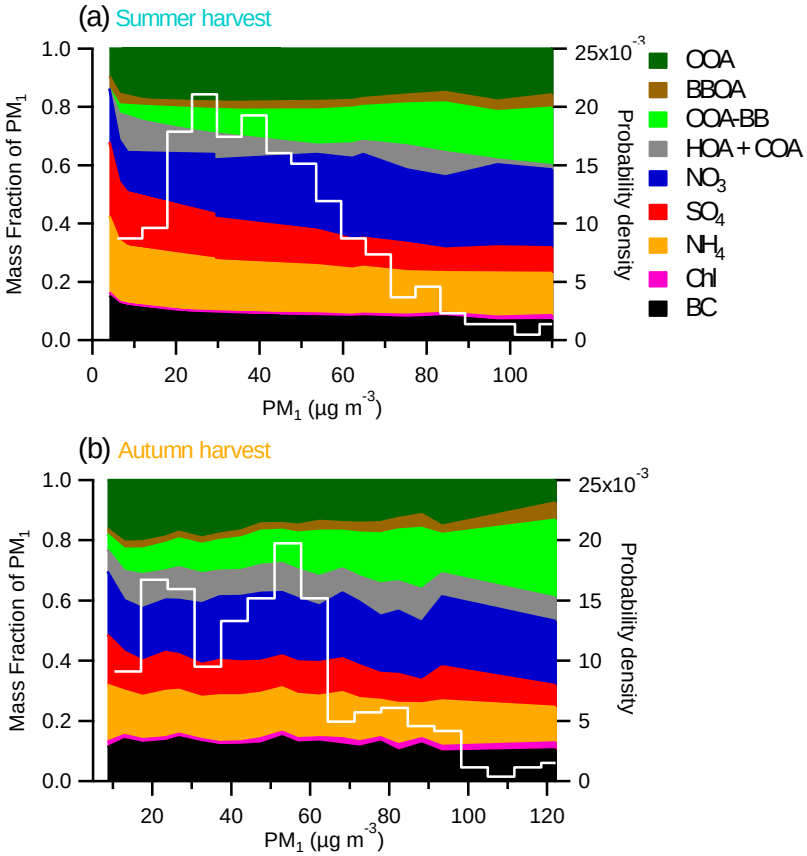

1053

1054 **Fig. 8.** The mass fractions of PM_1 species and OA components as a function of PM_1 mass loadings (left),

1055 and probability density of PM_1 mass loadings (right, with the white lines in the plots) during the summer

1056 and autumn harvest respectively.

1057

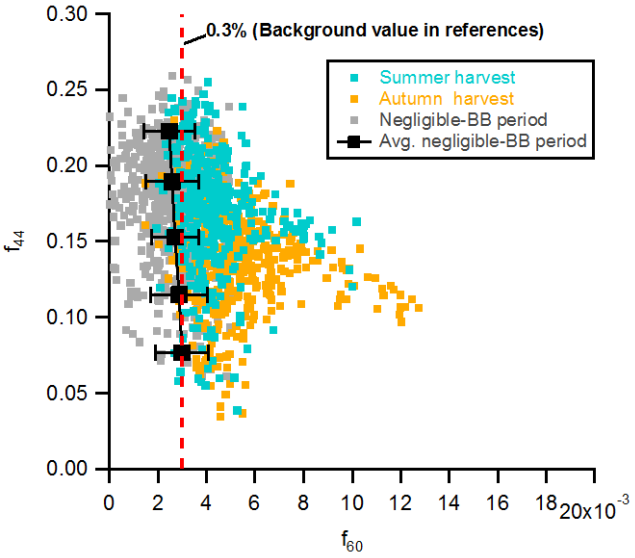

Fig. 9. Summary plots showing f_{44} vs. f_{60} for measurements with little or negligible biomass burning influence. Colored by the summer harvest (blue), autumn (orange) harvests, and little or negligible biomass burning influence period (gray, July 1 to 8, 2013), respectively. The presented background values of f_{60} (~0.26 ± 0.1%) in this study. Also shown is the average background level of f_{60} (~0.3%, red dashed line) in other studies from Aiken et al. (2009) and Cubison et al. (2011) for references.

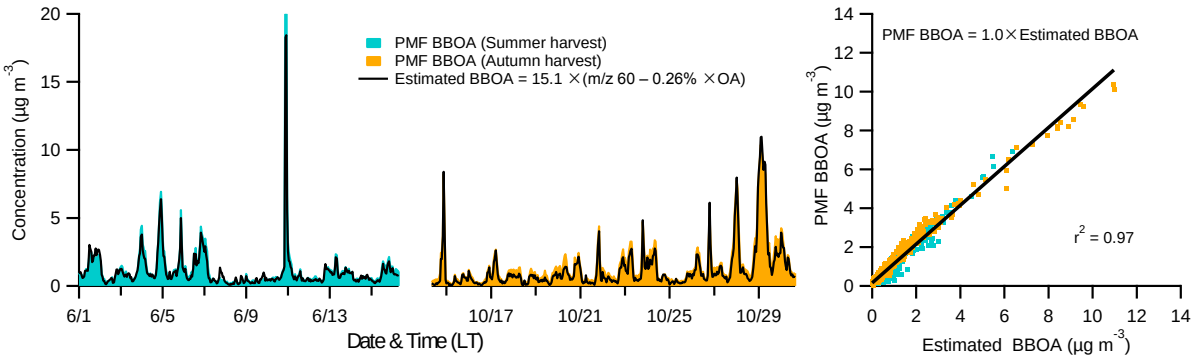

1065

1066 **Fig. 10.** Time series of BBOA identified by PMF (PMF BBOA) and estimated BBOA during the harvest

1067 seasons, as well as correlation plot of estimated BBOA vs. PMF BBOA. Note that the highest values for

1068 case 1 (Fig. 1c) during the summer harvest have been removed for fitting.

1069

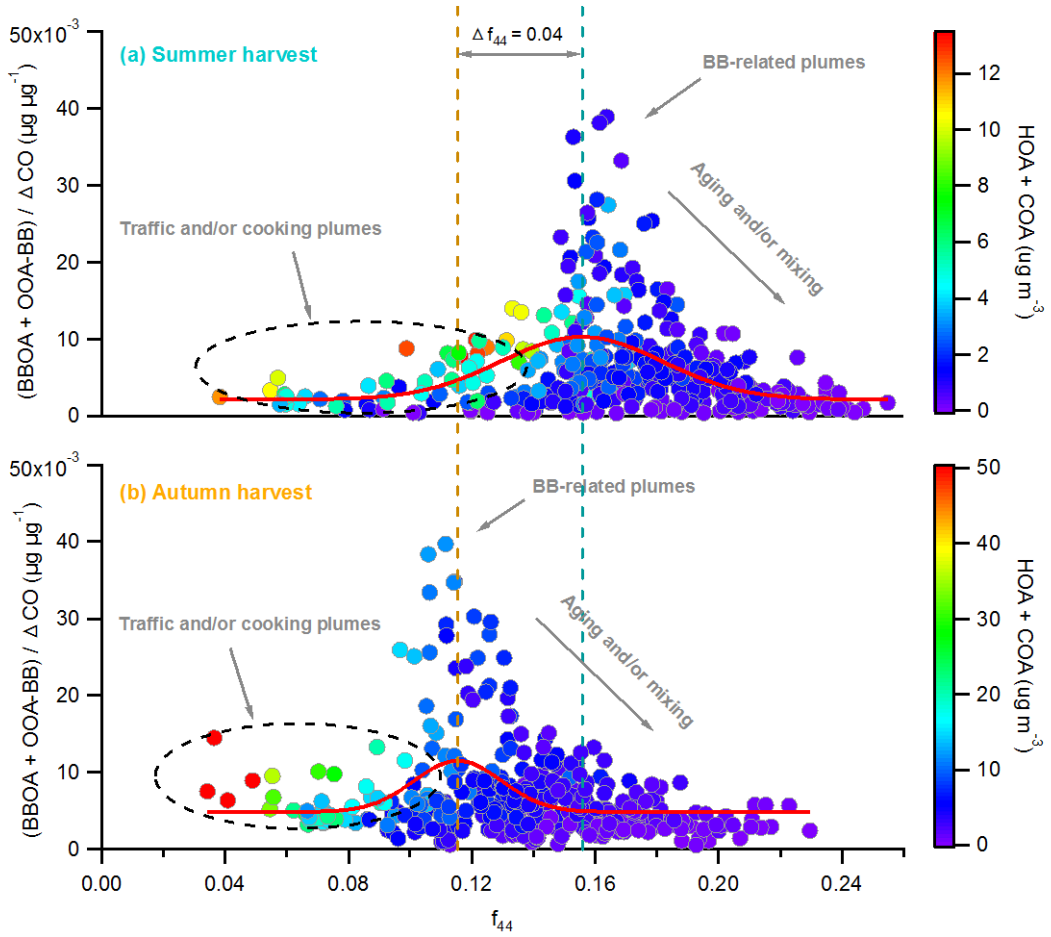

Fig. 11. The (BBOA + OOA-BB) / ΔCO ratio as a function of f_{44} during the summer and autumn harvest respectively. Colored by the HOA + COA mass concentrations, and the red curve lines are the Gaussian fitting for the summer and autumn harvest.

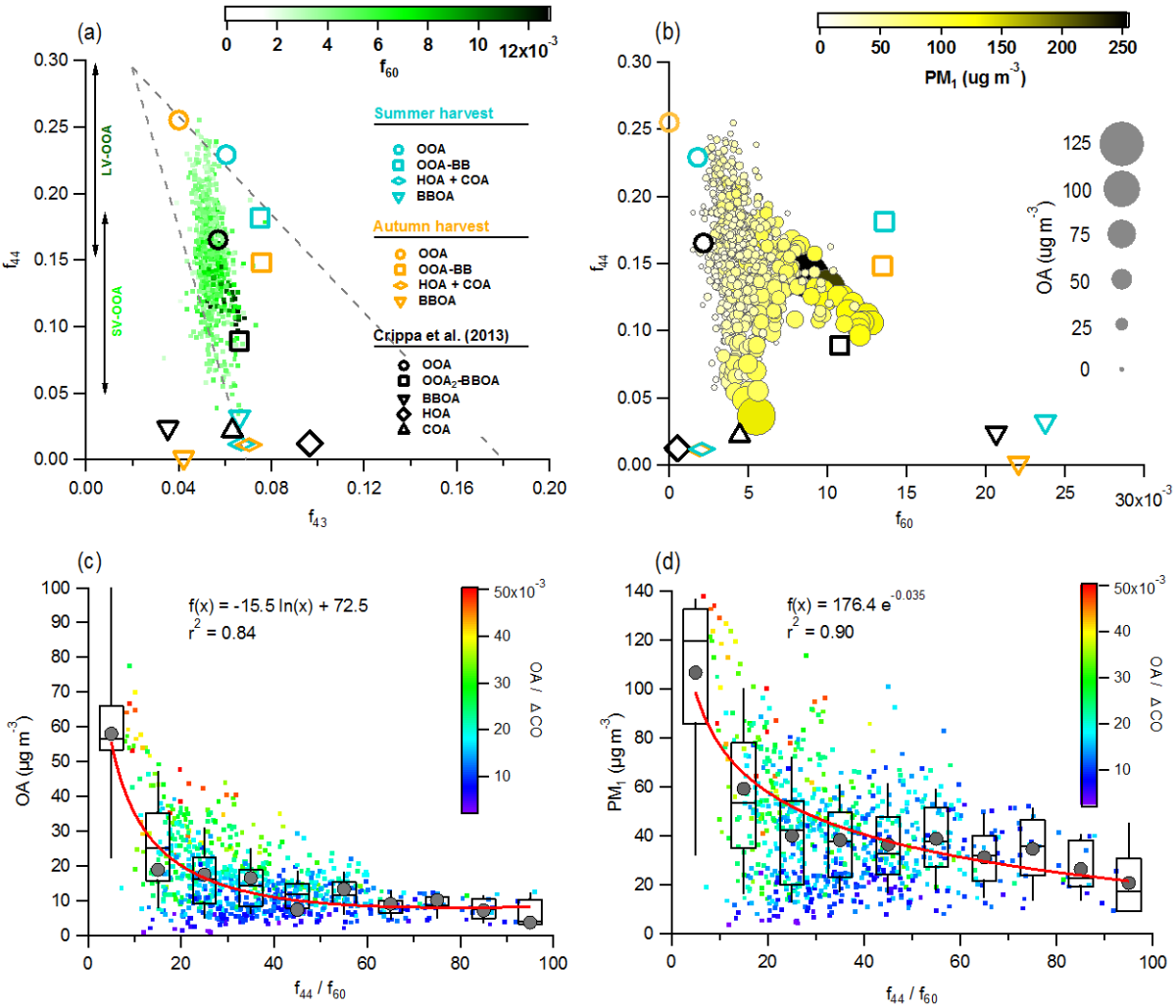

Fig. 12. Summary plots showing **(a)** triangle plot (f_{44} vs. f_{43}), SV-OOA and LV-OOA are represented for semi-volatile OOA and low-volatility OOA respectively. The dots are colored by f_{60} as a biomass-burning marker; **(b)** f_{44} as a function of f_{60} (f_{44} vs. f_{60}), colored by the PM_1 mass concentration and sized by the OA loadings; **(c - d)** the total OA and PM_1 mass concentration as a function of the ratio f_{44} / f_{60}, colored by the OA /ΔCO ratio, respectively. Here using the mean values (gray points) for curve fitting (c - d).

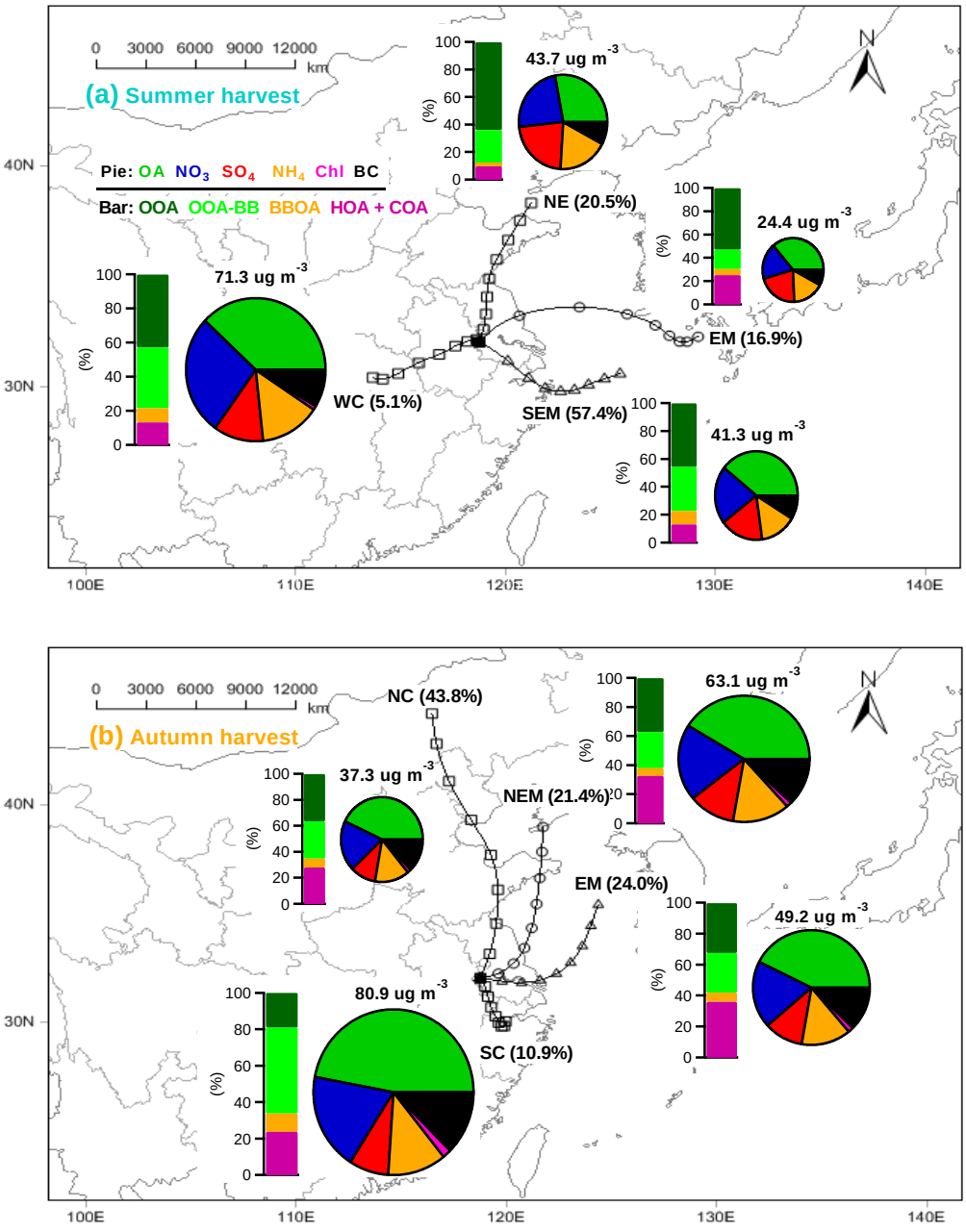

1082

1083 **Fig. 13.** Average composition of PM_1 (pie charts) and OA factors (bar charts) for each cluster. The four
1084 clusters are: **(a)** northeasterly (NE) back-trajectories (BTs), easterly marine (EM) BTs, southeasterly
1085 marine (SEM) BTs and westerly continental (WC) during the summer harvest; and **(b)** northerly
1086 continental (NC) BTs, northeasterly marine (NEM) BTs, easterly marine (EM) BTs and southerly
1087 continental (SC) during the autumn harvest. The markers on the trajectories indicate 6 h interval.